frontiers | Frontiers in Earth Science

TYPE Original Research
PUBLISHED 18 July 2025
DOI 10.3389/feart.2025.1553074

OPEN ACCESS

EDITED BY
Wenbin Tang,
Chengdu University of Technology, China

REVIEWED BY
Ruyue Wang,
State Key Laboratory of Shale Oil and Gas Enrichment Mechanisms and Efficient Development, China
Hongjian Zhu,
Yanshan University, China
Muhsan Ehsan,
Bahria University, Pakistan
Steven J. Schatzel,
Centers for Disease Control and Prevention (CDC), United States

*CORRESPONDENCE
Yi Hu,
✉ 1711409196@qq.com

RECEIVED 30 December 2024
ACCEPTED 19 May 2025
PUBLISHED 18 July 2025

CITATION
Yang L, Hu Y, Yang X, Zhang L, Tang W, Liu D, Li H, Wen Q, Xie L, Wang X, Kang J, Xi Z and Guo R (2025) Response of geochemical characteristics of organic-rich shale of Longmaxi formation to the sedimentary environment in the Neijiang-Rongchang area, Sichuan Basin, China.
Front. Earth Sci. 13:1553074.
doi: 10.3389/feart.2025.1553074

Response of geochemical characteristics of organic-rich shale of Longmaxi formation to the sedimentary environment in the Neijiang-Rongchang area, Sichuan Basin, China

Licheng Yang[1], Yi Hu[2]*, Xinrui Yang[1], Lianghua Zhang[1], Wen Tang[1], Dongxi Liu[1], Huilin Li[1], Qibing Wen[1], Lin Xie[2], Xingzhi Wang[2], Jiahao Kang[2], Zhidian Xi[2] and Ruiyu Guo[2]

[1]Chongqing Gas Field, PetroChina Southwest Oil and Gas Field Company, Chongqing, China, [2]State Key Laboratory of Oil and Gas Reservoir Geology and Exploitation, Southwest Petroleum University, Chengdu, China

The Lower Paleozoic (Upper Ordovician–Silurian), a globally deposited organic-rich shale, is one of the most prevalent source rocks worldwide. However, the origin of these shales remains uncertain. Here, this study reports geological and geochemical findings that present novel evidence for the origin of these shales. The mineral composition of Lower Silurian Longmaxi shale is dominated by quartz (average: 53.76%) and clay minerals (average: 33.37%). It constitutes a small amount of feldspar, calcite, dolomite, and pyrite. The Longmaxi Formation shale has high organic matter content (more than 2% on average). According to the geochemical indices, such as V/(V + Ni), Ni/Co., U/Th and Mo/total organic carbon (TOC), the Longmaxi Formation shale was deposited in the marine basin environment stranded by the sulphidation of anoxic water. Sensitive elements, such as Ba, Mo, P and Ti, indicate that although the primary productivity of the Longmaxi Formation shale remains low, it still has excellent source rock potential because of superior preservation conditions. A comparative study is conducted with the Lower Silurian hot shale in other parts of the world, it is found that the enrichment of organic matter in the Longmaxi Formation is controlled by high primary productivity (nutrients brought by upwelling) and strong preservation conditions (hypoxia caused by stratified water body), which subverts the traditional cognition of single main controlling factor. The organic matter enrichment of the Lower Silurian thermal shale has a ' productivity-preservation condition ' trade-off mechanism: low latitudes (such as North Africa) are dominated by high productivity. The middle and high latitudes (such as South China) are dominated by strong preservation conditions (limited basin sulfidation). It provides theoretical basis and motivation for future research and effectively guides the exploration and development of unconventional shale gas.

KEYWORDS

longmaxi formation, organic-rich shale, geochemical characteristics, sedimentary environment, sichuan basin

1 Introduction

Recent years have witnessed increased global exploration and advancement of unconventional shale gas (Bohacs et al., 2000; Curtis, 2002; Jarvie et al., 2007; Zhang et al., 2008; Zhang Q. et al., 2019; Aplin and Macquaker, 2011; Hao et al., 2011; Plint, 2014; Grygar et al., 2017; Potter, 2018; Liu et al., 2025). The Silurian shales are known as hot shales due to their elevated uranium concentration, making them highly radioactive (up to 400 API units), equating to approximately 3 wt% total organic carbon (TOC) (G. Konert, 2001; Lüning et al., 2000; Lüning et al., 2005; Mahmoud et al., 1992; Xia et al., 2024; Guo et al., 2024). Currently, more and more studies have confirmed the presence of hot shale gas potentials worldwide, such as the Sarchahan Formation in Iran, Qusaiba Formation in Saudi Arabia, Akkas Formation in Iraq, Mudawwara Formation in Jordan, Sahmah Formation in Oman, Tanf Formation in Syria, Dadas Formation in Turkey (Aqrawi, 1998; Brew et al., 1997; Sen and Kozlu, 2020), Longmaxi Formation in China (Zhang et al., 2008; Liang et al., 2012; Dai et al., 2014; Wang, 2015; Guo and Zhang, 2014; Guo, 2016; Zhao et al., 2023). Experts have estimated that the shale gas resources of the Longmaxi Formation in China's Sichuan Basin exceed 10 trillion cubic metres (Zhang, 2015; Jiang et al., 2023). Because the accumulation, formation mechanism and deposition process of the organic matter in Silurian hot shales are intricate, it is still a controversial and challenging research topic (Canfield, 1994; Rimmer et al., 2004). For further investigation, scholars around the globe have conducted a series of studies on the reconstruction of the paleo-environment from Late Ordovician to Early Silurian, integrating the disciplines of petrology, stratigraphy, palaeontology, palaeoclimatology, geochemistry and other areas. However, the understanding of the mechanism of sea level change and organic matter enrichment is different in different regions, and the sedimentary environment and geochemical analysis results are still debatable (Al-Ameri, 2009; Liu et al., 2019; Bartlett et al., 2018; Zhang et al., 2018; Smolarek et al., 2017; Bjerrum, 2018). Therefore, investigations of the consistency of geochemical indices and sedimentary facies in different regions are crucial for determining the sedimentary environment changes from Late Ordovician to Early Silurian (Jin, 2023; Zhao et al., 2024).

This research applied element geochemistry (major and trace elements), organic geochemistry (TOC), sedimentology and petrology methods to discuss the sedimentary environment change features of the Longmaxi Formation shale and the major controlling factors affecting the enrichment of organic matter. A comparative study is conducted with the Lower Silurian hot shale in other parts of the world, it is found that the enrichment of organic matter in the Longmaxi Formation is controlled by high primary productivity (nutrients brought by upwelling) and strong preservation conditions (hypoxia caused by stratified water body), which subverts the traditional cognition of single main controlling factor. It provides theoretical basis and motivation for future research and effectively guides the exploration and development of unconventional shale gas.

2 Geological setting

The Sichuan Basin in southwestern China (Figure 1A) is a sub-cratonic basin within the Yangtze Plate (Liang, 2015). The basin can be classified into five secondary tectonic units (Wang et al., 2019). The study region is situated in the low and gentle tectonic areas of central Sichuan (Figure 1A). In the Late Ordovician, the Yangtze Plate was located in the equatorial sea area on the northern margin of the Gondwana continent (He, 2020) (Figure 1A). From the Middle Ordovician through the Early Silurian, the episodic deformation of the Kwangsian movements (suturing of the Yangtze and Cathaysian blocks) affected the South China Craton during the Nanhua Basin closure process (Chen et al., 2014). The compression between the Yangtze block and the Cathaysian block to the southeast created a foreland basin next to the Wuyi–Yunkai orogenic belt (Chen et al., 2014; Charvet et al., 2010; Liu et al., 2017). Because of Kwangsian movements, several uplifts were developed as carbonate platforms on the periphery of the Upper Yangtze area, such as the Chuanzhong uplift on the northwestern side, the Qianzhong uplift on the southwestern side, the Xuefeng uplift on the southeastern side and the Yichang submarine paleohigh in the northeastern side (Chen et al., 2016; Lu et al., 2021).

Under the effects of transgression and tectonic activities, the black organic-rich shale of the Wufeng Formation was developed in the Late Ordovician of the Sichuan Basin, which has a thickness of about 5 m. It has high siliceous content and comprises ample graptolite, radiolarian, sponge spicules and other fossils (Lu et al., 2020; Hu et al., 2022; Wang et al., 2022). At the turn of the Late Ordovician and Early Silurian, the sea level dropped substantially due to the impact of the Hirnantian glaciation. A layer of biocrust limestone, "the Guanyinqiao section", with a thickness of about 1 m, was deposited in the Sichuan Basin, which is rich in benthic Hirnantian fauna (Ge et al., 2021; Gao et al., 2023). In the Early Silurian, deep-gray to black organic-rich shales of the Longmaxi Formation were widely deposited across the middle-upper Yangtze region, reaching a cumulative thickness of approximately 500 m. The lower Longmaxi Formation is dominated by siliceous shales (SiO_2 content: 60%–80%) exhibiting millimeter-scale horizontal laminae. These shales contain siliceous microfossils such as radiolarians and sponge spicules, indicative of biogenic silica accumulation under a deep-water shelf environment (Chen et al., 2024). Up-section, Caledonian tectonic uplift along the northern margin of the Yangtze Block triggered a paleogeographic transition from a deep-water shelf to a shallow shelf system (Zhu et al., 2024). This shift coincided with a progressive increase in sandy detritus (from 5% to 30%), marked by intercalated fine sandstone layers and silt-rich laminations (Figure 1C). Enhanced terrigenous input during this phase diluted biogenic sedimentation, resulting in a notable decline in graptolite fossil abundance (Liang et al., 2018). Additionally, multiple thin tuffaceous beds (2–10 cm thick) are interstratified within both the Wufeng and Longmaxi Formations (Figure 1B). Zircon U-Pb ages from these tuffs cluster at 445–440 Ma, correlating with Early Silurian volcanic arc activity in South China (Xu et al., 2022). Volcanic ash deposition likely stimulated primary productivity

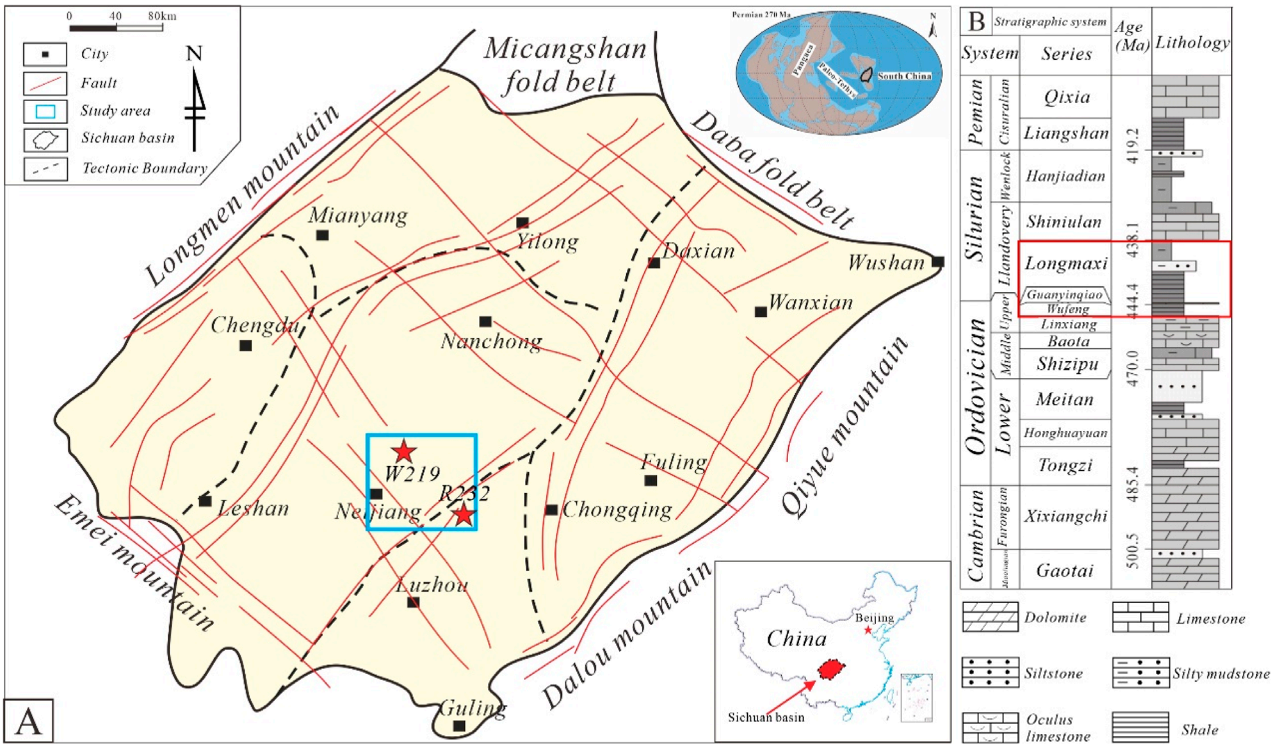

FIGURE 1
Regional geological structure map **(A)** (According to Wang et al., 2019) and stratigraphic column map **(B)** (According to Lu et al., 2020) of Sichuan Basin.

through the release of bioessential nutrients (e.g., Fe, P), leading to a 1%–2% increase in total organic carbon within adjacent sedimentary layers (Gao et al., 2023).

3 Petrological characteristics

The lithofacies of the Long1-1 sub-member of the Longmaxi Formation in the Neijiang-Rongchang region of the Sichuan Basin are primarily siliceous shale (Figures 2A, B, D, E), calcareous shale (Figure 2F) and silty shale (Figure 2C). The mineral components are essentially quartz, clay minerals, calcite, dolomite, feldspar and pyrite (Wang et al., 2021a). Taking Well Rong232 as an example, the quartz content is the highest, with a mass fraction of 22.67%–88.31% and an average of 53.76%. The exogenous quartz generated by the terrestrial input is irregularly angular, with a particle size of 20–50 μm (Figure 3A). Biogenic quartz (siliceous sponge spicules and siliceous radiolarians) has cryptocrystalline structure and a particle size of 50–200 μm (Figure 3B). The granular microcrystalline quartz is formed in the diagenesis stage, and the particle size is less than 20 μm (Figure 3B). The surface of quartz particles is wrapped by organic matter film, which inhibits the proliferation of secondary quartz (Figure 3G). The mass fraction of calcite is 1.32%–32.86%, with an average of 5.65%. It is mainly present as irregular granular or bright crystal calcite formed by diagenesis (Figures 3D, E). The mass fraction of dolomite is 1.40%–12.31%, with an average value of 6.69%, and it has a high self-shaped degree (Figure 3F). The average content of plagioclase is 1.55%–10.11%, with an average of 4.04%. The plagioclase is dominated by terrigenous input plagioclase, which is irregularly angular. It has a particle size of 20–50 μm and visible polybicrystals (Figure 3G). The mass fraction of clay minerals ranges from 21.33% to 47.45%, with an average of 33.37%. The clay minerals are essentially illite-montmorillonite mixed layer, illite and chlorite (Liu et al., 2023; Mao et al., 2024; Qin et al., 2024; Xiao, 2019; Liu et al., 2019) (Figure 3H). The mass fraction of pyrite is 1.30%–3.61%, with an average of 1.26%. It is present as strawberry-like pyrite aggregates and self-shaped particles (Figure 3I).

Siliceous shales are predominantly distributed in the Wufeng Formation and the lower part of the Longmaxi Formation, with a layered distribution and a thickness of 300 μm – 1 cm. The core colour is mostly black-grey black (Figures 2A, B, D, E), the hardness is generally relatively high and the TOC content is 4.03% on average. The siliceous shales in the study region have high siliceous content and complex sources, mainly including terrigenous, biogenic and diagenetic (autogenetic) (Han et al., 2024; Liu et al., 2023; Zhu et al., 2025). Previous studies on terrigenous origin and diagenesis have confirmed that quartz in the investigation area does not come from hydrothermal sources, and SiO_2 generated by clay mineral conversion largely creates granular microcrystalline quartz dispersed in the clay matrix (Xu et al., 2021; Yang et al., 2018; Zhu et al., 2024). The abundance of radiolaria, spongospicule and other fossils in the siliceous shale (Figure 3B) indicates that their biogenic origin is a partial dissolution of siliceous bioclasts (Mao et al., 2024; Qin et al., 2024; Xiao., 2019; Liu et al., 2019).

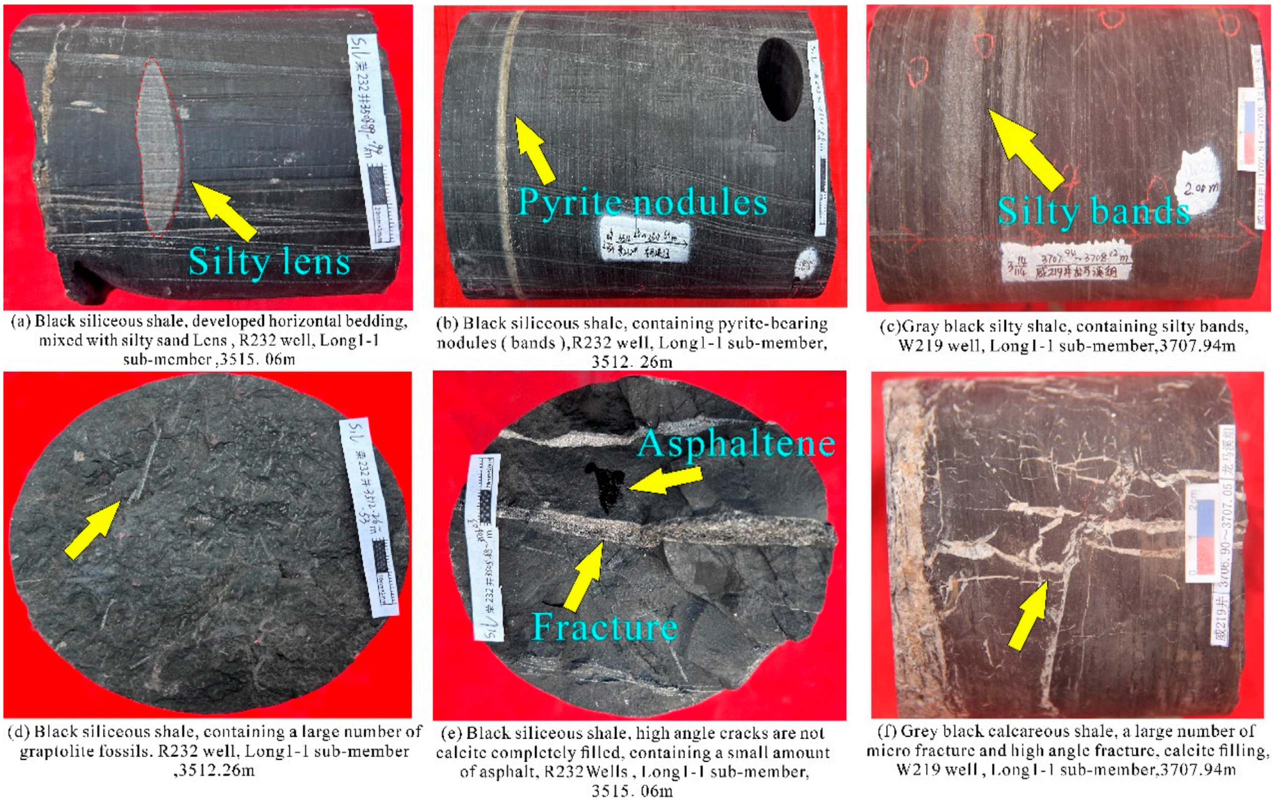

FIGURE 2
Core pictures of the Longmaxi formation long1-1 sub-member in the Neijiang-Rongchang area. **(a)** Black siliceous shale, developed horizontal bedding, mixed with silty sand Lens, R232 well, Long1-1 sub-member, 3515.06m. **(b)** Black siliceous shale, containing pyrite-bearing nodules (bands), R232 well, Long1-1 sub-member, 3512. 26m. **(c)** Gray black silty shale, containing silty bands, W219 well, Long1-1 sub-member.3707.94m. **(d)** Black siliceous shale, containing a large number of graptolite fossils. R232 well, Long1-1 sub-member ,3512.26m. **(e)** Black siliceous shale, high angle cracks are not calcite completely filled, containing a small amount of asphalt. R232 Wells. Long 1-1 sub-member,3515.06m. **(f)** Grey black calcareous shale, a large number of micro fracture and high angle fracture, calcite filling. W219 well, Long 1-1 sub-member.3707.94m

4 Samples and methods

The samples were collected from the Long1-1 sub-member of the Silurian Longmaxi Formation in Well R232 and Well W219 in the Sichuan Basin. The two wells are very representative wells in the Neijiang-Rongchang area. Among them, the shale gas production of R232 well is better, while the production of W219 is not as expected. The comparative study of the two wells can more intuitively show the impact of our findings on shale gas exploration and production. The two wells were sampled intensively every 1–2 m, and the number of samples per well was more than 40. Finally, representative samples were selected for conducting analyses and experiments according to the previously reported research findings of organic matter features and sedimentary environment. The representative samples meet the following requirements: they can reflect the main lithological characteristics of the target layer, the samples maintain the original structure, and are not affected by secondary effects such as weathering, oxidation or fluid intrusion, a sufficient number of samples to cover the variation range of the target layer. The representative analysis results of sampled shale can be referred to Table 1.

The thin section observation and scanning electron microscopy were performed at Southwest Petroleum University, Sichuan Key Laboratory of Natural Gas Geology of China. The experimental instrument is the Quanta650FEG field emission environment scanning electron microscope (SEM) of FEI Company. All samples were treated with argon ion polishing and gold spraying before SEM observation.

The total organic carbon test was carried out in Beijing Craton Company. The test instrument was Lectra CS744 carbon and sulfur analyzer. The test conditions were: room temperature 21°C, humidity 50%, atmospheric pressure 1,031 hPa, and the test standard was GB/T 19,145–2022.

The analysis of major and trace elements was completed in the Sedimentation Laboratory of Yangtze University in Jingzhou City, Hubei Province. The analytical instrument was Inductively Coupled Plasma - Atomic Emission Spectrometer (ICP-AES) Semmerfeld iCAP 7,000 series. The detection standard was GB/W 07,107. The sample preparation conditions were detailed as follows: the oven was set at 105°C, 0.30 g of lithium metaborate was evenly mixed with 0.05 g sample in a graphite crucible, the muffle furnace was set at 860°C and the melting time was 20 min. The beads were poured into 30 mL of 5% dilute nitric acid. The oscillator and shock were placed for 2 h until the molten salt was completely dissolved. Finally, it is filled with pure water to 100 mL (Zhang et al., 2002). During the sample analysis process, the use of standard and blank samples

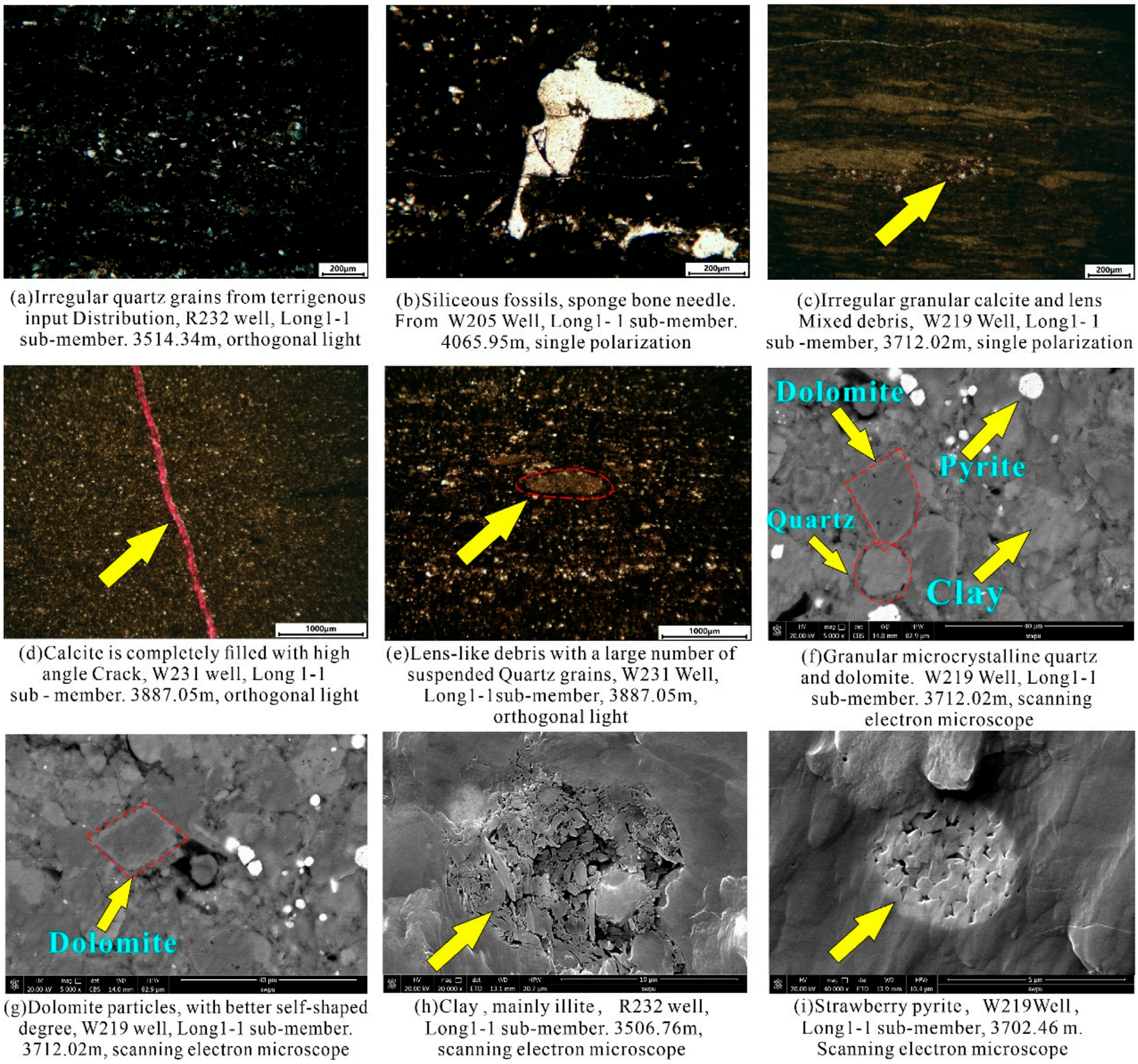

FIGURE 3
SEM - SE and SEM-BSE images, and transmitted light photomicrographs of mineral components in Long1-1 sub-member of Longmaxi Formation in the Neijiang-Rongchang area. **(a)** Irregular quartz grains from terrigenous input. Distribution, R232 well, Long1-1 sub-member. 3514.34m, orthogonal light. **(b)** Siliceous fossils, sponge bone needle. From W205 Well, Long1-1 sub-member. 4065.95m, single polarization. **(c)** Irregular granular calcite and lens Mixed debris, W219 Well, Long1-1 sub-member, 3712.02m, single polarization. **(d)** Calcite is completely filled with high angle Crack, W231 well, Long 1-1 sub member. 3887.05m, orthogonal light. **(e)** Lens-like debris with a large number of suspended Quartz grains, W231 Well, Long1-1 sub-member, 3887.05m, orthogonal light. **(f)** Granular microcrystalline quartz and dolomite. W219 Well, Long1-1 sub-member. 3712.02m, scanning electron microscope. **(g)** Dolomite particles, with better self-shaped degree, W219 well, Long1-1 sub-member. 3712.02m, scanning electron microscope. **(h)** Clay, mainly illite, R232 well, Long1-1 sub-member. 3506.76m, scanning electron microscope. **(i)** Strawberry pyrite, W219 Well, Long 1-1 sub-member, 3702.46 m. Scanning electron microscope.

can monitor instrument stability and evaluate data drift to ensure the accuracy and reliability of the data. In this element experiment, one standard was inserted into every 10 samples, and the deviation between the value of the standard and the recommended value was not more than 10%. Each batch of sample analysis contains at least one blank sample. The blank sample uses the same reagent and preparation process as the sample, and the blank value is less than 10% of the sample concentration. The above shows that the experimental detection is not subject to background interference or pollution, and the data is accurate and reliable.

The standardization of samples of Al elements derived from terrestrial sources and stable during diagenesis can quickly evaluate the different dilutions of sediments caused by the reduction of authigenic components of metal elements and carbonates in a large number of samples (Wedepohl, 1971; Tribovillard et al., 2006; Liu et al., 2019; Xiao, 2019). Table 2a enlists the test findings of

TABLE 1 The geological background of the selected representative samples.

Representative sample	Stratigraphic interface	Lithological description	Spatial variability
R232-13	The interface of the Wufeng Formation, the bottom is the Linxiang Formation, and the top is the Herantian stage	Siliceous shale, containing a large number of graptolite and other biological debris	Low TOC, and the mineral content is mainly siliceous
R232-19			
R232-17	The interface of Long1-1 sub-member, the bottom is Herantian stage, and the top is Long1-1 sub-member	Organic-rich siliceous shale, graptolite-bearing	High TOC, and the minerals are mainly siliceous and clay
R232-11			
W219-3			
W219-9			
W219-25			
W219-11			
R232-5	Long1-1 sub-member	Siliceous shale, clay shale, silty shale	TOC content decreased and silty increased
R232-15			
W219-13			
W219-19			
R232-9	The interface of Long1-1 sub-member, the top is Long1-2 sub-member	Clay shale, silty shale	Low TOC, silt increased
R232-3			
W219-21			
W219-27			
R232-1	Long1-2 sub-member	Silty shale	Low TOC decreases, and the mineral content is dominated by silt
R232-7			
W219-15			
W219-23			

organic carbon and major elements in the shale of the Wufeng-Longmaxi Formation. Table 2b presents the test results of trace elements. The formulas involved in this work are as follows:

$$X_{EF} = (X/Al)_{sample} * (X/Al)_{PAAS}$$

The Post-Archean Australian Shale (PAAS) represents the average component content of Palaeozoic to Cenozoic shales (Wedepohl, 1971; Taylor and McLennan, 1985).

5 Results

5.1 Organic matter abundance

In anoxic sedimentary environments (such as swamps and deep-sea sediments), when sulfate-reducing bacteria decompose organic matter (TOC), hydrogen sulfide (H_2S) and sulfide are generated, resulting in sulfur (S) enrichment. At this time, high TOC is often accompanied by high sulfur content, reflecting strong reduction conditions. In recent decades, C-S-Fe systematics have been widely used to assess paleoredox conditions in marine systems. (Algeo and Maynard, 2004). In TOC–S crossplots (Figure 4A), a “normal marine trend” with a slope of 0.4 was identified for modern oxic–suboxic environments by Berner and Raiswell, 1983.

The TOC content at the bottom of Long1-1 in the study area was 2.84–4.75%, with an average of 3.795%. The S content was 0.99–1.78%, with an average of 1.39%. The TOC content in the longitudinal direction gradually decreased. The TOC content in the middle of Long1-1 was 0.37–3.61%, with an average of 2.27%. Similarly, the S content was 0.95–2.01%, averaging 1.3%. From the top of Long1-1 to Long1-2, the S content gradually decreased and tended to be stable (Figure 4B). When TOC was 2%, the correlation between the TOC and S contents was weakened (Figure 4A) (Wang T. et al., 2020). Table 2a shows the geological context of representative samples.

TABLE 2 (a) Results of TOC and major element composition of the Long1-1 sub-member. (b) Content of trace elements and inorganic geochemical indices.

Sample	Depth	TOC/%	Major-element contents (wt%)											
			S/%	SiO_2	Al_2O_3	CaO	Fe_2O_3	K_2O	MgO	Na_2O	MnO	TiO_2	P_2O_5	Sum
(a)														
W219-1	3,686.97	0.17	0.12	64.15	16.79	0.65	5.31	3.56	2.81	0.39	0.03	0.54	0.09	99.03
W219-3	3,712.02	3.61	1.22	50.04	10.45	11.89	3.76	2.82	3.15	0.29	0.10	0.52	0.18	100.71
W219-5	3,702.46	0.83	0.83	60.93	16.98	0.59	6.22	4.17	3.03	0.31	0.06	0.56	0.09	99.25
W219-7	3,703.14	0.95	0.95	65.24	16.75	0.62	4.00	2.61	2.97	0.11	0.04	0.34	0.06	99.73
W219-9	3,712.39	3.33	1.50	47.49	10.06	14.37	4.01	2.65	3.21	0.28	0.11	0.51	0.27	101.35
W219-11	3,715.03	2.84	0.99	42.04	10.73	14.36	3.82	2.86	4.57	0.23	0.15	0.47	0.11	99.43
W219-13	3,709.6	3.58	1.30	45.56	9.41	12.31	3.70	2.54	5.07	0.27	0.16	0.47	0.41	99.50
W219-15	3,681.21	0.35	0.60	59.84	18.09	0.44	6.68	4.47	3.09	0.23	0.05	0.62	0.09	99.31
W219-17	3,704.1	1.62	1.20	60.65	17.21	0.27	6.60	4.33	3.10	0.37	0.05	0.62	0.10	100.60
W219-19	3,709.28	3.12	0.97	45.54	11.12	10.84	4.00	2.91	5.41	0.36	0.19	0.53	0.48	100.28
W219-21	3,706.54	0.37	2.01	44.31	28.59	0.46	8.98	5.97	2.32	0.78	0.00	0.95	0.08	100.94
W219-23	3,684.92	0.13	0.83	61.48	18.60	0.07	7.15	4.53	3.32	0.43	0.05	0.67	0.11	101.50
W219-25	3,715.23	4.75	1.78	48.79	11.81	8.52	5.40	3.06	4.61	0.31	0.11	0.56	0.22	100.77
W219-27	3,705.08	1.60	1.22	60.63	15.95	1.83	5.63	4.05	3.17	0.56	0.06	0.58	0.09	100.35
W219-29	3,687.21	0.25	0.47	60.64	19.39	0.77	6.65	4.71	3.28	0.45	0.05	0.61	0.11	101.55
R232-1	3,468.99	—	—	59.91	15.74	0.02	7.51	3.74	2.62	1.33	0.05	0.57	0.09	99.18
R232-3	3,506.76	—	—	57.67	16.44	2.21	5.01	4.03	2.95	1.03	0.03	0.65	0.11	99.62
R232-5	3,514.34	—	—	63.19	16.11	1.94	4.39	3.81	2.48	1.53	0.03	0.58	0.10	101.16
R232-7	3,479.81	—	—	59.93	16.90	0.65	6.65	4.05	3.14	0.99	0.06	0.57	0.10	99.65
R232-9	3,484.56	—	—	58.21	14.73	3.66	5.78	3.56	3.72	1.07	0.12	0.56	0.09	100.90
R232-11	3,536.73	—	—	69.07	9.87	1.62	3.41	2.57	2.25	0.66	0.03	0.46	0.11	99.55
R232-13	3,537.67	—	—	51.24	14.32	5.99	5.64	3.71	3.63	0.55	0.11	0.35	0.11	99.25
R232-15	3,524.82	—	—	62.20	12.35	3.81	3.84	2.78	2.73	1.54	0.04	0.57	0.11	100.48
R232-17	3,527.78	—	—	74.63	7.47	1.52	2.43	1.96	1.81	0.51	0.03	0.30	0.07	99.53
R232-19	3,540.57	—	—	68.68	11.84	0.24	4.97	3.11	1.69	0.44	0.06	0.63	0.07	99.43

Sample	Trace element content/($\mu g^* g^{-1}$)													
	V	Cu	Co.	Ni	Th	U	Mo	Sr	Ba	V/(V + Ni)	Ni/Co.	U/Th	Sr/Ba	Sr/Cu	Cu/Al
(b)															
W219-1	111.18	96.23	12.40	40.06	0.32	2.67	0.07	28.45	241.53	0.74	3.23	8.2	0.12	0.30	10.88
W219-3	242.91	78.61	13.31	82.22	0.31	14.83	1.59	167.58	394.94	0.75	6.18	48.0	0.42	2.13	14.28

(Continued on the following page)

TABLE 2 (*Continued*) (a) Results of TOC and major element composition of the Long1-1 sub-member. (b) Content of trace elements and inorganic geochemical indices.

Sample	Trace element content/($\mu g^* g^{-1}$)														
	V	Cu	Co.	Ni	Th	U	Mo	Sr	Ba	V/(V + Ni)	Ni/Co.	U/Th	Sr/Ba	Sr/Cu	Cu/Al
W219-5	126.12	28.93	13.36	40.13	0.24	3.15	0.46	25.68	204.46	0.76	3.00	13.0	0.13	0.89	3.23
W219-7	108.87	27.43	15.02	40.00	0.24	3.60	0.52	52.83	273.59	0.73	2.66	14.8	0.19	1.93	3.11
W219-9	166.85	64.82	10.89	65.93	0.26	9.82	0.82	172.80	320.37	0.72	6.05	37.6	0.54	2.67	12.23
W219-11	258.08	53.08	11.21	69.62	0.28	15.58	1.38	157.76	373.08	0.79	6.21	55.4	0.42	2.97	9.39
W219-13	301.94	55.15	7.98	73.20	0.24	10.76	1.08	123.73	306.80	0.80	9.17	45.4	0.40	2.24	11.12
W219-15	130.54	5.52	24.54	50.42	0.34	3.32	0.09	22.08	256.87	0.72	2.05	9.7	0.09	4.00	0.58
W219-17	117.26	58.63	15.95	34.79	0.30	5.39	0.76	18.02	232.57	0.77	2.18	18.3	0.08	0.31	6.47
W219-19	335.24	70.68	10.85	97.28	0.31	11.42	1.29	160.81	410.19	0.78	8.96	36.9	0.39	2.28	12.07
W219-21	6.65	5.05	1.07	10.54	0.45	8.18	0.27	12.28	273.27	0.39	9.84	18.3	0.04	2.43	0.34
W219-23	141.39	9.96	25.74	60.57	0.41	3.88	0.14	95.39	319.87	0.70	2.35	9.5	0.30	9.58	1.02
W219-25	286.91	141.00	16.13	113.28	0.27	16.90	2.18	134.60	354.98	0.72	7.02	63.5	0.38	0.95	22.66
W219-27	156.47	37.29	16.37	70.98	0.30	6.31	1.03	60.00	256.86	0.69	4.34	21.2	0.23	1.61	4.44
W219-29	144.65	8.62	21.02	49.30	0.37	3.40	0.11	27.75	244.59	0.75	2.35	9.2	0.11	3.22	0.84
R232-1	133.23	46.01	12.90	64.03	0.24	5.92	1.05	44.86	825.88	0.68	4.96	25.1	0.05	0.98	5.55
R232-3	110.20	37.02	11.29	54.12	0.22	7.10	1.32	76.08	470.60	0.67	4.79	32.3	0.16	2.06	4.27
R232-5	81.65	21.34	10.99	31.71	0.31	7.01	1.14	102.53	575.07	0.72	2.88	22.5	0.18	4.80	2.51
R232-7	216.08	48.62	15.61	56.72	0.33	6.77	0.73	35.11	514.29	0.79	3.63	20.8	0.07	0.72	5.46
R232-9	190.57	76.60	12.34	53.59	0.29	6.93	0.81	129.80	604.18	0.78	4.34	24.0	0.21	1.69	9.87
R232-11	157.28	77.67	10.80	70.10	0.22	16.27	1.89	101.01	516.63	0.69	6.49	73.0	0.20	1.30	14.94
R232-13	80.82	66.63	10.68	52.43	0.25	8.59	0.48	185.01	793.55	0.61	4.91	34.4	0.23	2.78	8.83
R232-15	104.09	14.84	9.34	48.50	0.26	7.92	1.33	133.12	548.55	0.68	5.20	31.0	0.24	8.97	2.28
R232-17	114.49	39.87	9.65	51.84	0.21	14.15	1.64	109.56	613.95	0.69	5.37	68.3	0.18	2.75	10.13
R232-19	179.81	120.85	13.90	73.54	0.36	9.40	1.98	14.56	487.04	0.71	5.29	26.3	0.03	0.12	19.37

5.2 Major element characteristics

The primary components of the Longmaxi Formation Long1-1 sub-member shale in the Neijiang-Rongchang area are SiO_2 (42.04%–74.63%, average: 57.68%), Al_2O_3 (7.47%–28.59%, average: 14.71%) and CaO (0.02%–14.37%, average: 3.99%). The total content of the three components was as high as 67%–84%. In addition to these three primary components, there is a small amount of Fe_2O_3, K_2O, MgO, Na_2O, MnO and other components (Table 2a).

Apparent differences were present in the content of major elements between the bottom layer and the upper layer of the Long1-1 sub-member. The SiO_2 content was low (average: 46.25%), and the CaO content was high (10.39%) in the bottom layer of Well W219. The SiO_2 content increased (average: 61.70%), and the CaO content sharply decreased (0.66%) in the top layer. The SiO_2 content in the bottom section of the R232 well was higher (average 64.84%), and the SiO_2 content in the top section was reduced (average 58.93%). The CaO content in the whole section was lower, with an average of 2.52% at the bottom and 1.64% at the top (Figure 5).

6 Discussion

6.1 Paleoredox conditions

The redox condition is affected by many factors, and a single index will have great uncertainty when revealing the redox state (Zhang et al., 2017). The research method of this paper integrates multiple indicators to comprehensively invert the redox situation, which can reduce the uncertainty of a single indicator, significantly reduce the interference of diagenesis, and improve the reliability of the reduction paleoenvironment (Chen et al., 2024; Han et al., 2024). Trace elements, such as V/(V + Ni), Ni/Co. and U/Th, are extensively used to identify ancient redox conditions (Dill, 1986; Tribovillard et al., 2006; Kimura, 2001; Hatch and Leventhal, 1992; Jones and Manning, 1994; Rimmer et al., 2004). Compared with Ni, V will preferentially precipitate from the sulphide environment. Hence, a sulphide-rich environment is formed when V and Ni are enriched simultaneously. The change of the V/(V + Ni) ratio also indicates the relative change of oxygen (Hatch and Leventhal, 1992). Demonstrated a significant correlation between the degree of pyrite mineralisation and the V/(V + Ni) ratio. Jones and Manning proposed that a Ni/Co. ratio greater than 7.0 corresponds to a reducing environment. A ratio between 5.0 and 7.0 suggests the existence of an oxygen-poor environment, and a value less than 5.0 indicates an oxygen-rich environment. "Th" is an element that is not easy to migrate in the low-temperature surface environment and is enriched in weathering-resistant minerals. In fine-grained sediments, "Th" is a component of heavy minerals or clay. "U" is easily precipitated as a tetravalent state in the reducing environment; thus, the U/Th ratio can reflect the redox conditions of the sedimentary water. When the U/Th ratio is high, the reducibility of seawater is stronger. A value greater than 1.25 indicates a reducing environment, 0.75–1.25 corresponds to an oxygen-poor environment, and less than 0.75 indicates an oxygen-rich environment (Table 3).

From the V/(V + Ni) ratio, the whole section (0.61–0.95) of Long1-1 in the W219 well and R232 well is suggested as a reducing environment. The following description provides the bottom data of the Long one to one subsection from well W219 3,706 m–3,715 m. The top data of well R232 is from W219 3,687 m–3,690 m and R232 3,485 m–3,480 m. The Ni/Co. ratio at the bottom of the Long1-1 sub-member (W219 is 7.63 on average, R232 is 5.45 on average) indicates a reduced or hypoxic environment. The Ni/Co. ratio at the top of the first sub-member of Long1-1 has a significant decreasing trend (W219 average is 2.77, R232 average is 4.12), indicating the weakening of reducibility. The U/Th ratio indicated a reducing environment (8.2–73.0) in the whole Long1-1. However, a significant downward trend is observed from the bottom (W219 was 47.8 on average and R232 was 50.5 on average) to the top (W219 was 12.99 on average, R232 was 4.92 on average) of the Long1-1, indicating that the upward reducibility is weakened, which is consistent with the Ni/Co. ratio.

In summary, the redox conditions of the Long1-1 in the Neijiang-Rongchang area did not change much during the sedimentary history, and the oxygen-poor-reducing environment was dominant. At the bottom of the Longmaxi Formation, the degree of reduction of the water body was relatively high, originating from the static marine environment containing certain sulphides. Later, local shock variations were observed in the redox environment in the upper part of the Longmaxi Formation, but they are basically in a stable state, which is the reduction environment (Figure 6; Figure 7).

6.2 Paleoproductivity

Ba, Mo, Cu, P, Ti, Al and other elements are the most widely used indicators of ancient marine productivity (Lu et al., 2021). A high concentration of SO_4^{2++} ions is created by H_2S oxidation (reoxidised) on the rotten organic matter surface, which will precipitate with Ba^{2+} in seawater. For this reason, barite ($BaSO_4$) content in high productivity areas is generally high (Wei, 2012). It is generally believed that when the content of Ba_{XS} is 1,000–5,000 μg/g, it has high productivity in the sedimentary environment (Wei, 2012). In oxidised-suboxidised water, Mo exists in the form of stable ions. In oxidising and sub-oxidising water, Mo is co-precipitated with the hydroxide of Mn, whereas, in anoxic water, MoO_4^{2-} is reduced to positive quaternary MoO^{2+}. Due to the good sulphophilicity of Mo, when a certain amount of H_2S is present in the water, the sulphide solid solution will strongly absorb Mo and react with it to form $MoO_{4-x}S_x^{2-}$ adsorbed on the humus/organic matter surface to generate autogenic precipitation enrichment. Therefore, Mo is a good indicator of anoxic sulphide water (Zhou et al., 2011; Erickson and Helz, 2000). Cu can be retained in sediments as organometallic complexes, and phosphorus (P) is an important part of organisms. The Cu/Al and P/Ti ratios are often used as indicators of paleoproductivity. In general, P/Ti values >0.79, 0.34 and 0.79, and <0.34 indicate high, medium, and low productivity, respectively (Algeo and Rowe, 2012).

The average content of Ba in the Long1-1 is low, but it cannot be determined that the paleoproductivity was low during the sedimentary period. There are two reasons for this phenomenon: 1. Sulphate ions in $BaSO_4$ may be reduced by vulcanising bacteria in an oxygen-poor anaerobic environment, resulting in a large amount of dissolution of $BaSO_4$ and loss of a part of biological Ba (Wei et al., 2021); 2. In the middle of the Wufeng Formation and the bottom of the Longmaxi Formation, there were two acts of biological extinction events in which a large number of organisms were wiped out, resulting in a low biological barium content in the Long1-1 sub-member shale formed in an oxygen-poor and anaerobic environment (Li et al., 2021).

In summary, the contents of Ba, Mo, Cu/Al and P/Ti in the Long1-1 of the Neijiang-Rongchang area have the same variation characteristics (Figure 6; Figure 7). In general, each index demonstrates that the paleoproductivity of the Long1-1 sub-member is not high, which is related to the deep-sea environment of anaerobic sulphide at that time. However, the paleoproductivity at the bottom of the Long1-1 was higher than that at the top of the Long1-1 and gradually decreased from bottom to top, which is consistent with the TOC test results and paleo-redox environment.

6.3 Palaeoclimate

Paleoclimatic conditions can be identified based on the changes in the content and ratios of Sr and Cu. The Sr element can be easier to deposit under dry conditions, and the Cu element

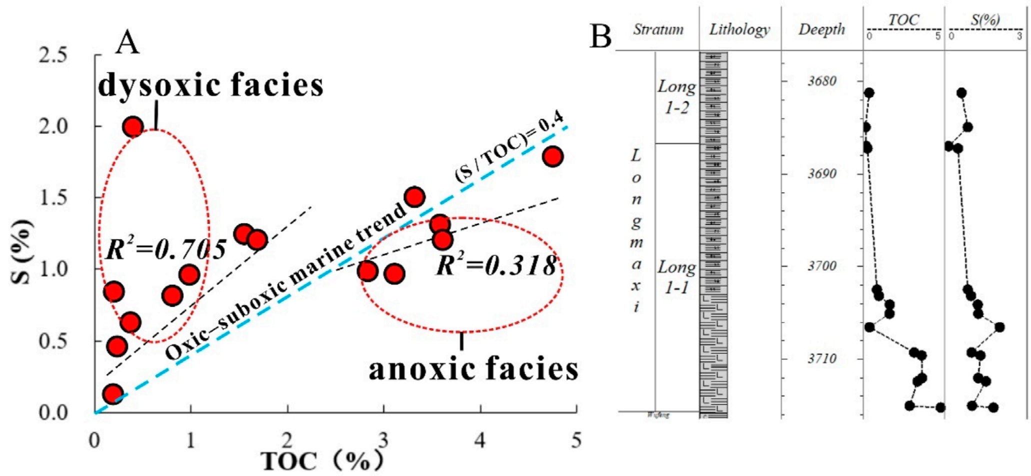

FIGURE 4
TOC and S element characteristic diagram of W219 well. **(A)** TOC and S element correlation diagram; **(B)** The variation characteristics of TOC and S elements.

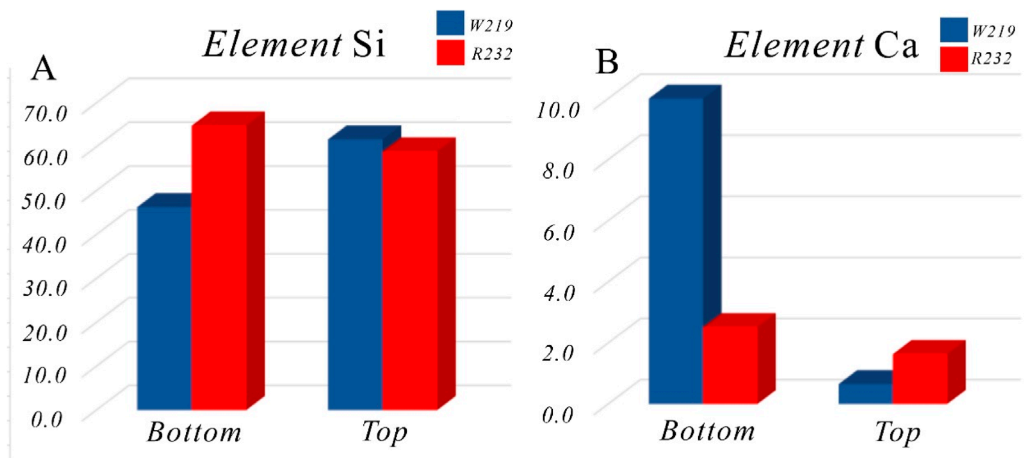

FIGURE 5
Characteristics of major elements in the Long1-1 sub-member. **(A)** The longitudinal variation characteristics of Si element; **(B)** The longitudinal variation characteristics of Ca element.

can be better preserved in a humid environment. Therefore, the increase in the Sr/Cu ratio indicates a drier paleoclimatic condition. It is generally believed that a Sr/Cu value greater than five indicates a dry-hot climate, whereas a value smaller than five suggests a wet-hot environment (Lerman, 1978). The Sr/Cu ratios of the samples in the study area were distributed in a large range (0.12–9.58, with an average of 2.77), indicating the hot climate conditions with fluctuating dry and wet conditions (Table 3).

The Sr/Cu value at the bottom of the Long1-1 was also small (W219 was 1.96 on average, and R232 was 2.75 on average). It can be speculated that after the Hirnantian glacial period, large-scale transgression occurred in the study area. Consequently, the climate became warm and humid. The Sr/Cu value was relatively stable in the middle of the Long1-1, and the R232 well exhibited a local increase (average: 6.89). These results indicate that the climate has become relatively dry and hot, which may be related to the sea level rise at that time (Han et al., 2024; Liu et al., 2023). In parallel, from the top to the top of the Long1-1, the Sr/Cu value gradually decreased, indicating that the climate became relatively warm and humid, which may be related to the decline of sea level at that time. The Sr/Cu value of the Long1-2 sub-member has an overall upward trend, and the paleo-climate is drier and hotter than that of the Long1-1 sub-member. This finding is consistent with the background of the convergence of the Pangea supercontinent and the gradual decline of global sea level at that time (Torsvik and Cocks, 2013). The relative sea level in the study area displayed a general downward trend with the gradual strengthening of the upward movement in Guangxi (Zou et al., 2018; Chen et al., 2014; Xu and Du, 2018).

TABLE 3 Element discrimination parameters of ancient sedimentary environment.

Paleoredox environment	Reducing Environment	Hypoxic environment	High oxic environment	Sources of indicator data
V/(V + Ni)	>0.60	0.45–0.60	<0.45	Tribovillard et al. (2006)
Ni/Co.	>7.0	7.0–5.0	<5.0	Jones and Meaning. (1994)
U/Th	>1.25	1.25–0.75	<0.75	Dill. (1986)
Ancient productivity	Sample Mean	High ancient productivity	Low ancient productivity	
Ba	204.46–825.88/423.85	>1,000	<1,000	Wei H.Y. (2012)
Mo	0.074–2.18/0.979	—	—	Brumsack (1986)
Cu/Al	0.34–22.66/8.11*10^{-4}	—	—	Wei et al. (2021)
P/Ti	0.07–0.71/0.22	>0.79	<0.34	Algeo and Rowe (2012)
Paleo-climate		Hot and dry climate	Warm and humid climate	
Sr/Cu	0.12–9.58/2.77	>5	<5	Lerman (1978)
Paleo-salinity		Marine saltwater	Onshore fresh water	
Th/U	0.1–0.12/0.05	<2	>2	Tan (2017)
Sr/Ba	0.03–0.54/0.22	>1	<1	Wang et al. (1979)

In summary, the paleo-climate in the study area from the bottom of the Long one to one to the bottom of the Long one to two experienced warm-humid-relative, dry-hot-warm-humid-relative and dry-hot stage changes.

6.4 Palaeosalinity

Under the influence of different weathering stability, the "Th" element is more likely to be adsorbed and remain in clay than the U element, which can be easily oxidised and leached. Generally, the Th/U ratio equals 2 as the boundary to identify the marine and continental strata. Among them, a value bigger than two indicates a continental freshwater deposition, whereas a value smaller than two corresponds to a marine saltwater deposition (Tan, 2017). Compared with Sr, Ba has a weaker migration ability in water. When the salinity of water increases, the development of $BaSO_4$ rather than Sr^{2+} is more favourable, leading to precipitation. At this time, the residual Sr element in water is gradually enriched. When the salinity increases to a certain extent, $SrSO_4$ increases and precipitates. Therefore, the Sr/Ba ratio has a good positive correlation with the salinity of ancient water, which can be used for the discrimination of ancient salinity (Wang et al., 2017; Wen et al., 2008; Wang A. L. et al., 2021).

Taking well W219 as an example, the Th/U value in the study area was between 0.1 and 0.12, with an average value of 0.05, indicating a marine saltwater sedimentary environment. The Th/U value gradually increased from the bottom to the top of the Long1-1, suggesting that the paleosalinity gradually decreased. The Sr/Ba value was low; however, it is stated as continental fresh water (presumably caused by late diagenesis). This result depicts a significant decreasing trend from the bottom to the top of the Long1-1 and indicates a gradual reduction in paleosalinity, consistent with the Th/U value (Table 3). Therefore, it can be concluded that the paleosalinity of Long1-1 in the Neijiang-Rongchang area is a marine environment of brackish water-saline water and gradually decreased from the bottom to the top, which is consistent with the paleo-climate, paleoproductivity and paleo-redox environment.

6.5 Degrees of seawater limitation

Using the previous discriminant plate of Mo–TOC water retention degree (Algeo and Lyons, 2006; Brumsack, 1986; Baturin, 2011; Piper and Dean, 2002), Figure 8A shows that the Mo/TOC value of the shale in the study area is generally less than 4.5, displaying a strong retention environment. This conclusion is basically consistent with the previously reported assumption that the sedimentary water body of the Wufeng Formation-Longmaxi Formation shale in the Sichuan Basin is a stagnant environment (Ran et al., 2015; Chen et al., 2016; Ma et al., 2016; Li et al., 2017; Nie et al., 2017). The Mo-U covariation model can not only be used to determine the redox index of water but also identify the water retention and redox conditions of the basin (Algeo and Lyons, 2006; Algeo and Tribovillard, 2009; Tribovillard et al., 2012; Westermann et al., 2013; Zhou et al., 2014). Figure 7B shows that the enrichment coefficient of Mo and U in shale is low. Furthermore, the Mo/U ratio is also low, which is only 0.1–0.3 times that of normal seawater, concentrated in the area of poor oxygen-anaerobic environment. With the increase in the TOC content, the reduction

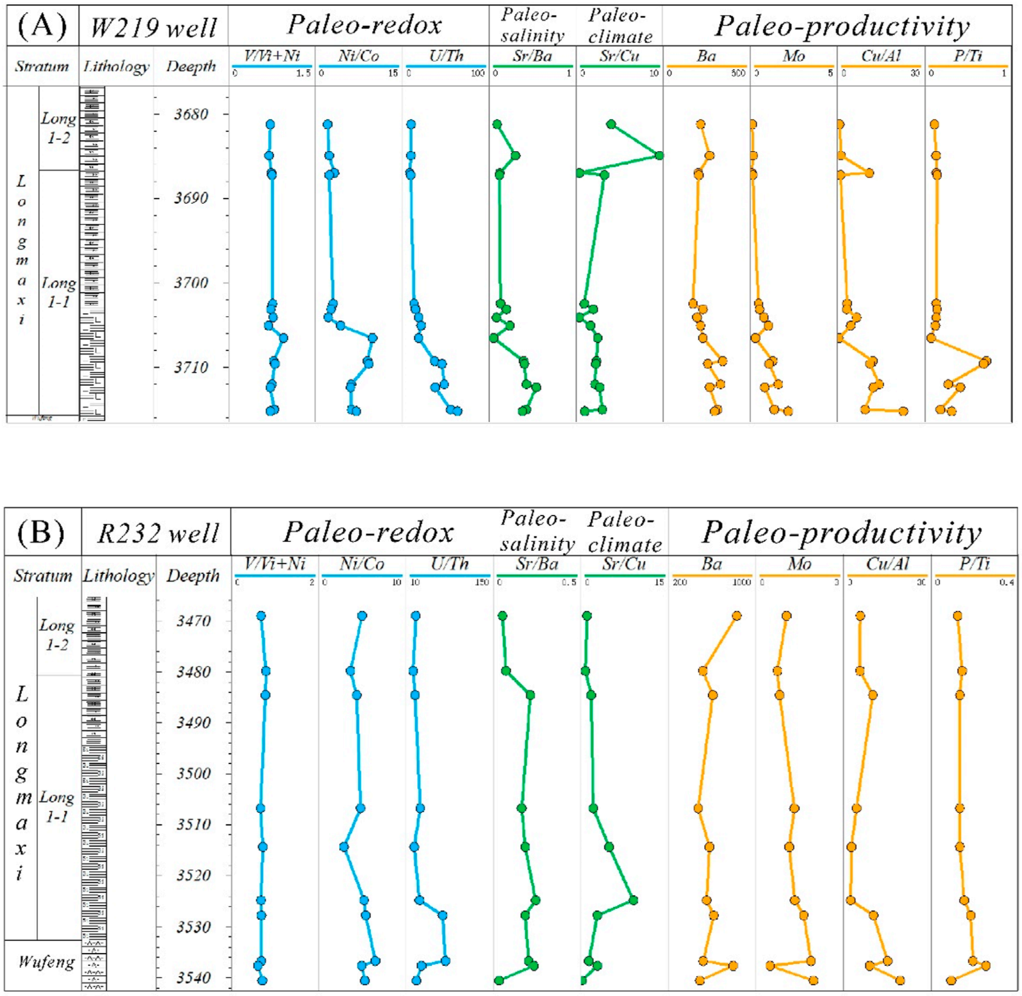

FIGURE 6
Evolution paleo-environmental characteristics of the sedimentary environment in well W219 **(A)** and well R232 **(B)**.

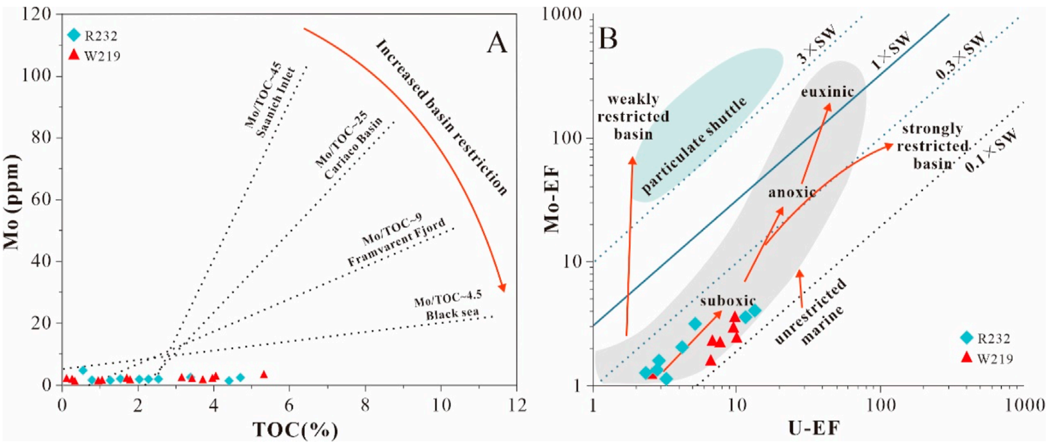

FIGURE 7
(A) Comparison of the Mo–TOC relationship for Wufeng and Longmaxi Formation in Sichuan Basin and those for modern anoxic basins (modified from Tribovillard et al., 2012). **(B)** U [EF] *versus* Mo [EF] covariation for Wufeng-Longmaxi Formation shales in Sichuan Basin (modified from Algeo and Tribovillard, 2009; Algeo and Lyons, 2012).

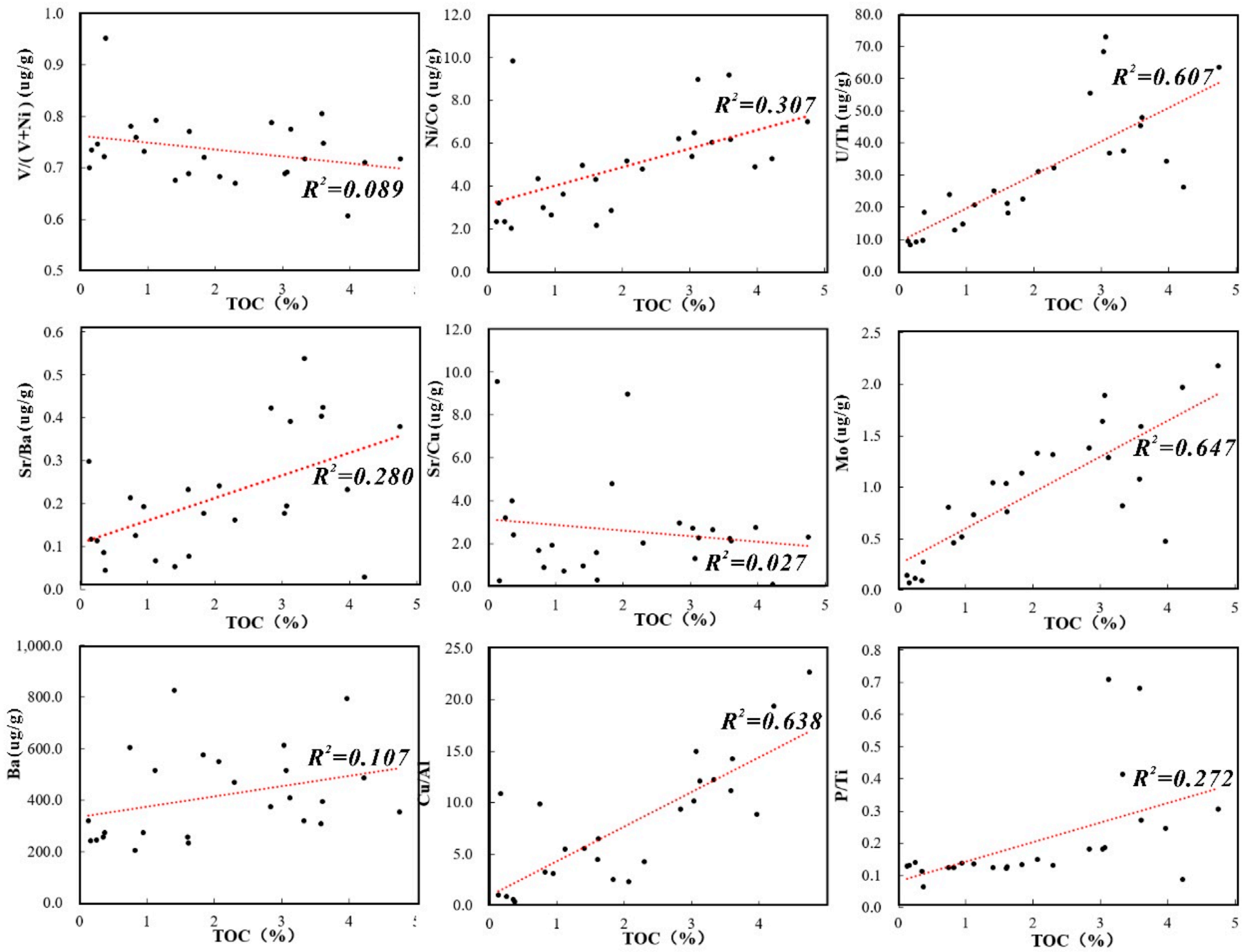

FIGURE 8
Correlation between TOC and geochemical indicators.

degree of water body became stronger. Notably, the enrichment of the Mo element was slower than that of U, leading to the change of Mo/U ratio from 0.3 × SW in anoxic-anaerobic environment to close to 0.1 × SW. These characteristics are basically consistent with the oxygen-poor-anaerobic environment of the modern strong retention basin (Tang et al., 2019).

In summary, it can be considered that the organic-rich shale in the Wufeng Formation-Longmaxi Formation Long1-1 of the Neijiang-Rongchang Block is created in an oxygen-poor-anaerobic strong retention basin environment, which is consistent with the conclusion of the Mo/TOC ratio.

6.6 Main controlling factors of organic shale enrichment

Paleo-environment restoration shows that the bay system in the study area is complex due to rich palaeontological content, which makes the sedimentary period of the Wufeng-Longmaxi Formation have a high paleo-productive background (Wei et al., 2021; Han et al., 2024; Liu et al., 2023). The paleoproductivity parameters Mo, Ba, Cu/Al and P/Ti correlate with TOC (Figure 8), consistent with the revealed background of high productivity at the bottom of Long1-1. Paleoredox environmental indicators Ni/Co. and U/Th were significantly correlated with TOC, whereas no significant correlation was found in V/(V + Ni), which may be attributed to diagenesis (Rimmer S.M., 2004). The TOC content has no significant correlation with the parameter reflecting paleo-climate (Sr/Cu) (Figure 8), suggesting that paleo-climate may not have substantial control over organic matter enrichment in marine sedimentary environments (Han et al., 2024). The correlation between the paleosalinity parameters (Sr/Ba) and TOC indicates that the paleosalinity of the marine sedimentary environment exerts a certain control effect on the enrichment of organic matter.

According to the sedimentary environment, diagenetic history, sea level changes and tectonic conditions, we believe a high TOC content must fulfil both the "productivity model" and the "preservation condition model". High primary productivity provides a large material base. The seawater's degree of anoxia and limitation regulate whether the organic matter can be deposited and enriched. For example, during the Hirnantian glaciation, the formation of glaciers caused global sea level to fall. Despite the abundance of benthic organisms, the water became an oxidising environment that was not conducive to preserving organic matter, generating

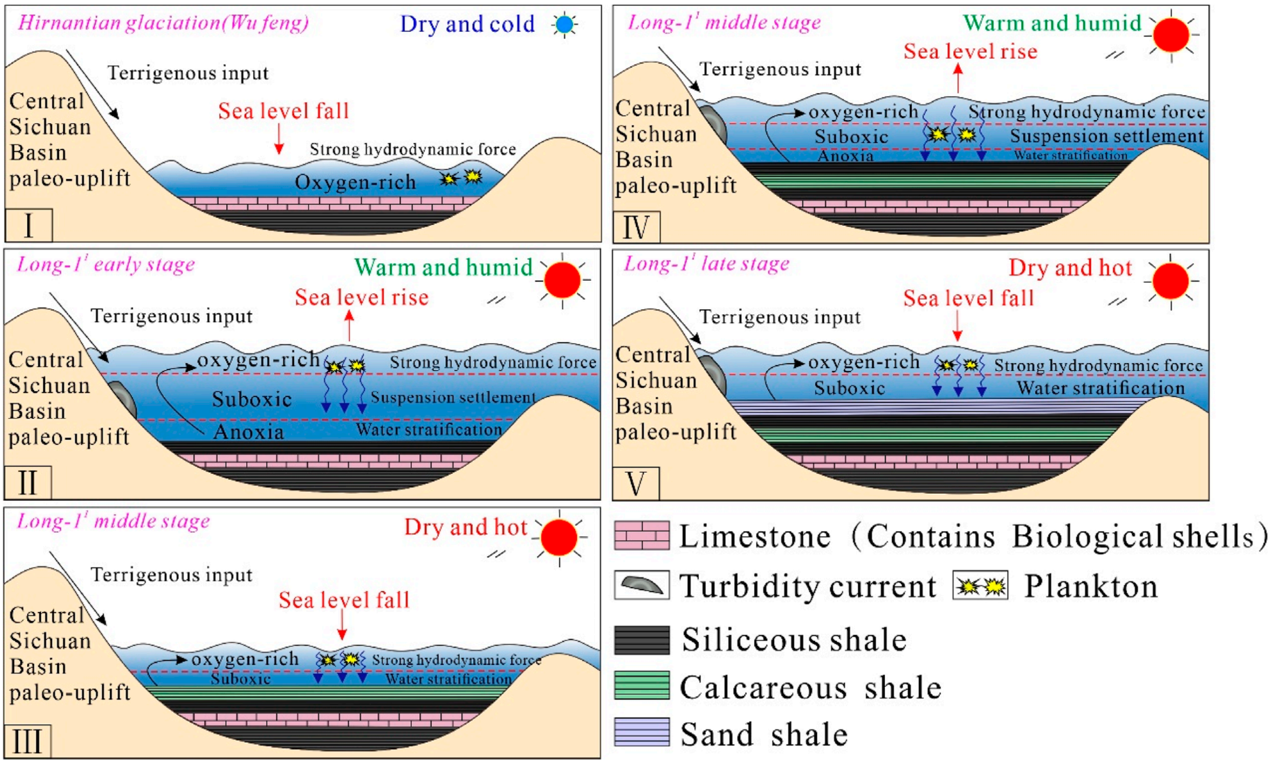

FIGURE 9
Sedimentary model of Wufeng Formation-Longmaxi Formation in Neijiang-Rongchang area of Sichuan Basin (modified from Han et al., 2024).

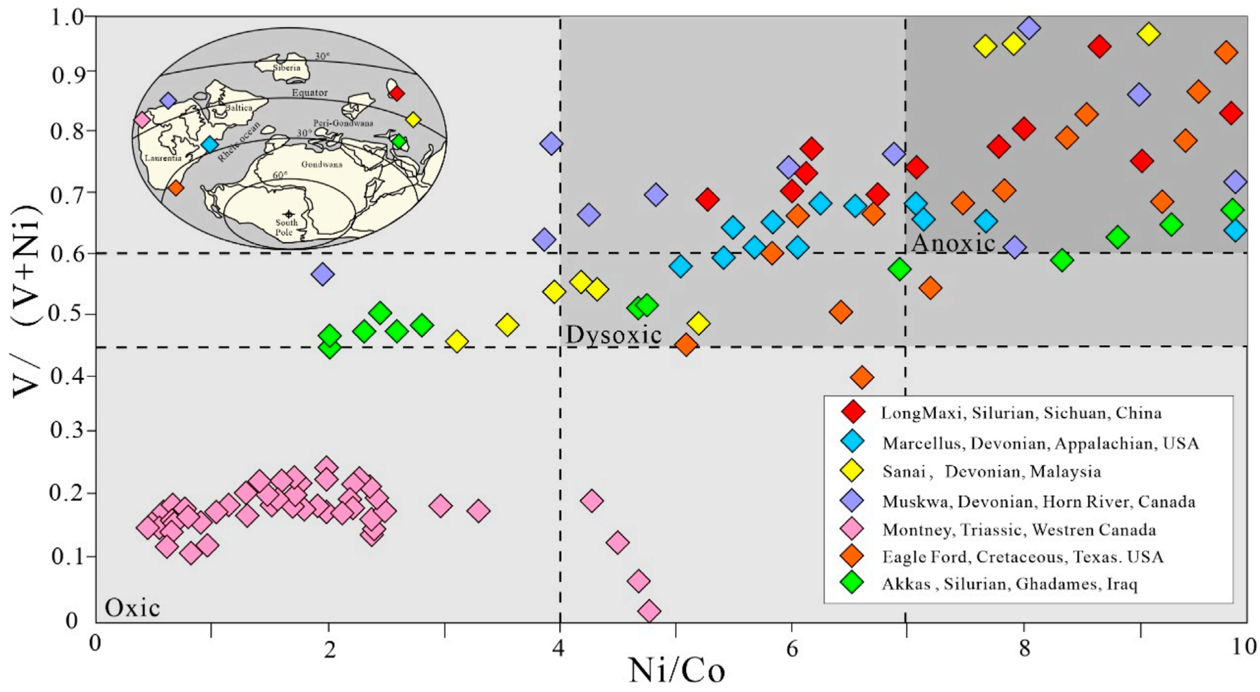

FIGURE 10
Comprehensive comparison diagram of redox index (The data in the figure are from French et al., 2019; Ibad and Padmanabhan, 2020; Agbogun et al., 2024; Al-Juboury et al., 2021; Ross and Bustin, 2009; Chen et al., 2015).

low TOC content. During the sedimentary period of the Longmaxi Formation, although the paleoproductivity was low, the reduced water environment and strong closure were good preservation conditions for organic matter, resulting in a high TOC content (Qiu et al., 2017; Wang et al., 2024; Huang et al., 2021).

The paleo-climate rapidly warmed during the Silurian period. Thus, the ice sheet rapidly melted (Figure 9I). The melting ice water entered the sea and caused a large increase in the volume of seawater, causing large-scale transgression (Han et al., 2024; Liu et al., 2023). This transgression stage is consistent with the global transgression boundary at the beginning of Silurian (Mao et al., 2024; Zhang L. C. et al., 2019). The rise in sea level caused the sea basin to expand in the region, and the water body became deeper and more anoxic, creating an anaerobic (still sea phase) environment containing H_2S. The paleo-climate became warm and humid, the redox-sensitive elements were strongly enriched, and the ratios of V/(V + Ni), Ni/Co., and U/Th were high, resulting in better preservation of organic matter. This effect induced the diffusion of seawater through the barrier, yielding the enhancement of the circulation between the sea basin and the ocean, the relative weakening of the retention degree of the sea basin, and the dominant redox conditions in the marine system (Figure 9II) (Han et al., 2024; Liu et al., 2023). Subsequently, the sea level slowly decreased, the climate became relatively hot and dry, and the supply of continental margin debris gradually increased. Even sandy debris was input, which was consistent with the increasing trend of Al_2O_3 and TiO_2 content. Consequently, the anoxic environment at the bottom was destroyed, and the salinity of seawater decreased with the decrease in the depth. The sea basin changed from the anaerobic environment at the bottom of the Longmaxi Formation to the normal oxygen-rich environment, which was not conducive to preserving organic matter. The low content of Mo, U, V, Ni, Co. and Cr, and the ratio of Th/U and Sr/Ba, which represented the paleosalinity, are a good indication for the manifestation of these effects (Figure 9III). Subsequently, the sea level slowly rose and remained high for a long time. The climate was warm and humid, the water retention was weak, and the reduction of bottom seawater was enhanced. Moreover, the paleosalinity of seawater slightly decreased, and the paleoproductivity relatively increased (Figure 9IV). At the top of Long one to one, the paleo-climate became warm and dry, and the sea level slightly decreased and tended to be stable. The reducibility of seawater also gradually weakened, the paleosalinity of the water body decreased and tended to be stable, and the paleoproductivity decreased (Figure 9V).

According to the above geochemical characteristics, the paleoproductivity and reduction conditions form a positive feedback, which determines the enrichment efficiency of organic matter in the study area. In addition, the paleoclimate can affect the supply of salinity and nutrients by controlling weathering and sea level changes; paleosalinity can regulate water stratification and redox state. Changes in the type and quantity of graptolites are ‘natural recorders’ of paleoenvironmental evolution (Nie et al., 2017). Multi-factor coupling analysis is the core of shale high-quality hydrocarbon source rock prediction in the future, and a comprehensive model needs to be constructed by combining multiple disciplines such as geochemistry, mineralogy and paleontology (Zhao et al., 2024; Xia et al., 2024).

The organic-rich intervals of the Long one to one submember are widely distributed in the Sichuan Basin and have good continuity in lateral distribution, which is of great significance for identifying the effective intervals of high and over mature marine shales. Also, it provides the basis of element geochemistry for predicting shale gas ‘sweet spot’. Along with the abundance of organic matter, other factors affecting the properties of the reservoir include brittleness, pore type, porosity, permeability and gas bearing (Wang et al., 2021b). Generally, the better shale brittleness, the stronger the fracture-forming ability and the better the transformation effect (Zhang et al., 2016; Zou et al., 2022). The content of brittle minerals in Long1-1 sub-member siliceous shale is extremely high, the organic matter pores are very developed, and the connectivity is good (Wang et al., 2018; Wang R. Y. et al., 2020). Overall, the Long1–1 sub-member siliceous shale can be used as a good reservoir due to its high abundance of organic matter, high content of brittle minerals, high porosity, permeability and gas bearing (Wang et al., 2021c; Liu et al., 2023).

6.7 Comparison with other cases worldwide

The depositional model of the Longmaxi Formation shales exhibits distinctiveness within global shale systems, characterized by tectono-sedimentary coupling mechanisms, volcanic influences, and post-depositional modifications that differ markedly from other shale deposits (Chen et al., 2015). However, the Longmaxi shale also exhibits similar inorganic geochemical characteristics to other shales in the world, including the Marcellus Shale in the Appalachian Mountains (Chen et al., 2015), the EagleFord Shale in Texas (French et al., 2019), the Sanai Shale in Malaysia (Ibad and Padmanabhan, 2020), the Muskwa Shale in Horn River, Canada (Ross and Bustin, 2009), the Montney shale in western Canada (Agbogun et al., 2024), and the Akkas Shale in the Ghadames Basin in Iraq (Al-Juboury et al., 2021). Using redox-sensitive elements (V, Co. and Ni), this study discovered that, in addition to Montney shale in western Canada, other shales and Longmaxi shale were in a continuous anoxic marine environment during the deposition period (Figure 10). There is a short-term oxygen/hypoxia boundary shift near the sediment-water interface. Due to provenance and tectonic background, the paleo-climate, paleosalinity and water retention degrees differ in different regions. We referred to the previous viewpoint that redox can be used as one of the reliable parameters to assess the reservoir potential in future research.

7 Conclusion

(1) The Long1-1 sub-member of the Longmaxi Formation in the Neijiang-Rongchang area is dominated by siliceous shale. It has high organic matter content. Moreover, this sub-member has radiolaria, spongosphora and other siliceous biological fossils; the rest are small amounts of calcareous shale, silty shale, etc.
(2) During the sedimentary period of the Longmaxi Formation, although the paleoproductivity was low, the reduced water

environment and strong sealing feature were excellent conditions for preserving organic matter. The results demonstrating a high TOC value of the black shale prove that the black of the Longmaxi Formation has a huge shale gas resource potential.

(3) The geochemical characteristics of the black shale in the Longmaxi Formation reflect its marine deep-water shelf sedimentary environment. The anoxic environment and high productivity are the main controlling factors for the development of high-quality shale, and regional tectonic and paleoclimatic events further affect the organic matter enrichment model. These understandings provide a scientific basis for shale gas exploration target interval optimization and resource evaluation.

Data availability statement

The raw data supporting the conclusions of this article will be made available by the authors, without undue reservation.

Author contributions

LY: Writing – original draft, Writing – review and editing. YH: Writing – original draft, Writing – review and editing. XY: Writing – review and editing, Funding acquisition. LZ: Writing – review and editing, Funding acquisition. WT: Writing – review and editing, Funding acquisition. DL: Writing – review and editing, Funding acquisition. HL: Writing – review and editing, Funding acquisition. QW: Writing – review and editing, Funding acquisition. LX: Writing – review and editing, Project administration. XW: Writing – review and editing, Validation. JK: Writing – review and editing, Investigation. ZX: Writing – review and editing, Investigation. RG: Writing – review and editing, Investigation.

Funding

The author(s) declare that no financial support was received for the research and/or publication of this article.

Conflict of interest

Authors LiY, XiY, LZ, WT, DL, HL, and QW were employed by PetroChina Southwest Oil and Gas Field Company.

The remaining authors declare that the research was conducted in the absence of any commercial or financial relationships that could be construed as a potential conflict of interest.

Generative AI statement

The author(s) declare that no Generative AI was used in the creation of this manuscript.

Publisher's note

All claims expressed in this article are solely those of the authors and do not necessarily represent those of their affiliated organizations, or those of the publisher, the editors and the reviewers. Any product that may be evaluated in this article, or claim that may be made by its manufacturer, is not guaranteed or endorsed by the publisher.

References

Agbogun, H. M., Wüst, R. A., Adeboye, O. O., and Nassichuk, B. (2024). Elemental geochemistry insights into source inputs, paleo-productivity, and paleo-depositional conditions of the Montney Formation. *Appl. Geochem.* 170, 106079. doi:10.1016/j.apgeochem.2024.106079

Al-Ameri, T. K. (2009). Palynostratigraphy and the assessment of gas and oil generation and accumulation in the Lower Paleozoic, Western Iraq. *Arab. J. Geosci.* 3, 155–179. doi:10.1007/s12517-009-0060-2

Algeo, T. J., and Lyons, T. W. (2006). Mo—total organic carbon covariation in modern anoxic marine environments: implications for analysis of paleoredox and paleohydrographic conditions. *Paleoceanography* 21 (1), 279. doi:10.1029/2004pa001112

Algeo, T. J., and Maynard, J. B. (2004). Trace-element behavior and redox facies in core shales of Upper Pennsylvanian Kansas-type cyclothems. *Chem. Geol.* 206 (3-4), 289–318. doi:10.1016/j.chemgeo.2003.12.009

Algeo, T. J., and Rowe, H. (2012). Paleoceanographic applications of trace-metal concentration data. *J. Chem. Geol.* 324, 6–18. doi:10.1016/j.chemgeo.2011.09.002

Algeo, T. J., and Tribovillard, N. (2009). Environmental analysis of paleoceanographic systems based on molybdenum–uranium covariation. *Chem. Geol.* 268 (3-4), 211–225. doi:10.1016/j.chemgeo.2009.09.001

Al-Juboury, A. I., Hussain, S. H., and Al-Lhaebi, S. H. (2021). Geochemistry and mineralogy of the Silurian Akkas Formation, Iraqi western desert: implications for palaeoweathering, provenance and tectonic setting. *Arabian J. Geosciences* 14, 760–823. doi:10.1007/s12517-021-06887-w

Aplin, A. C., and Macquaker, J. H. S. (2011). Mudstone diversity: origin and implications for source, seal, and reservoir properties in petroleum systems. *AAPG Bull.* 95. 2031, 2059. doi:10.1306/03281110162

Aqrawi, A. A. M. (1998). Paleozoic stratigraphy and petroleum systems of the western and Southwestern Deserts of Iraq, GeoArabia 3(2). *Apr.* 1998), 229. doi:10.2113/geoarabia0302229

Bartlett, R., Elrick, M., Wheeley, J. R., Polyak, V., Desrochers, A., and Asmerom, Y. (2018). Abrupt global-ocean anoxia during the Late Ordovician-early Silurian detected using uranium isotopes of marine carbonates. *Proc. Natl. Acad. Sci. U. S. A.*, 20, 115 (23), 5896–5901. doi:10.1073/pnas.1802438115

Baturin, G. N. (2011). Geochemistry of sapropel in the black sea. *Geochem. Int.* 49 (5), 531–535. doi:10.1134/s0016702911050028

Berner, R. A., and Raiswell, R. (1983). Burial of organic carbon and pyrite sulfur in sediments over Phanerozoic time: a new theory. *Geochimica Cosmochimica Acta* 47 (5), 855–862. doi:10.1016/0016-7037(83)90151-5

Bjerrum, C. J. (2018). Sea level, climate, and ocean poisoning by sulfide all implicated in the first animal mass extinction. *Geology* 46 (6), 575–576. doi:10.1130/focus062018.1

Bohacs, K. M., Carroll, A. R., Neal, J. E., and Mankiewicz, P. J. (2000). Lake basin type, source potential, and hydrocarbon character: an integrated sequence-stratigraphic geochemical framework. *AAPG Bull.* 46, 3–33.

Brew, G. E., Litak, R. K., Seber, D., Barazangi, M., Al-Imam, A., and Sawaf, T. (1997). Basement depth and sedimentary velocity structure in the northern Arabian platform, eastern Syria. *Geophys. J. Int.* 128 (3), 617–631. doi:10.1111/j.1365-246X.1997.tb05323.x

Brumsack, H. J. (1986). The inorganic geochemistry of Cretaceous black shales (DSDP Leg 41) in comparison to modern upwelling sediments from the Gulf of California. *Spec. Publ.* 21 (1), 447–462. doi:10.1144/gsl.sp.1986.021.01.30

Canfield, D. E. (1994). Factors influencing organic carbon preservation in marine sediments. *Chem. Geol.* 114 (3-4), 315–329. doi:10.1016/0009-2541(94)90061-2

Charvet, J., Shu, L., Faure, M., Choulet, F., Wang, B., Lu, H., et al. (2010). Structural development of the Lower Paleozoic belt of South China: genesis of an intracontinental orogen. *J. Asian Earth Sci.* 39 (4), 309–330. doi:10.1016/j.jseaes.2010.03.006

Chen, C., Mu, C. L., Zhou, K. K., Liang, W., Ge, X. Y., Wang, X. P., et al. (2016). The geochemical characteristics and factors controlling the organic matter accumulation of the late Ordovician—early Silurian black shale in the upper Yangtze basin, south China. *Mar. Petroleum Geol.* 76, 159–175. doi:10.1016/j.marpetgeo.2016.04.022

Chen, R., Sharma, S., Bank, T., Soeder, D., and Eastman, H. (2015). Comparison of isotopic and geochemical characteristics of sediments from a gas-and liquids-prone wells in Marcellus Shale from Appalachian Basin, West Virginia. *Appl. Geochem.* 60, 59–71. doi:10.1016/j.apgeochem.2015.01.001

Chen, X., Fan, J., Chen, Q., Tang, L., and Hou, X. (2014). Toward a stepwise kwangsian orogeny. *Sci. China Earth Sci.* 57, 379–387. doi:10.1007/s11430-013-4815-y

Chen, Y. C., Lin, W., Li, M. T., Han, D. L., and Guo, W. (2024). The distribution and main controlling factors of high-quality shale in Longmaxi Formation in southern Sichuan-eastern Sichuan Region. *Special Oil and Gas Reservoirs* 31 (4), 54–63. doi:10.3969/j.issn.1006-6535.2024.04.007

Curtis, J. B. (2002). Fractured shale-gas systems. *AAPG Bull.* 86 (11), 1921–1938. doi:10.1306/61eeddbe-173e-11d7-8645000102c1865d

Dai, J., Zou, C., Liao, S., Dong, D., Ni, Y., Huang, J., et al. (2014). Geochemistry of the extremely high thermal maturity Longmaxi shale gas, southern Sichuan basin. *Org. Geochem*. 74, 3–12. doi:10.1016/j.orggeochem.2014.01.018

Dill, H. (1986). Metallogenesis of early paleozoic graptolite shales from the graefenthal horst (northern bavaria-Federal Republic of Germany). *Econ. Geol.* 81 (4), 889–903. doi:10.2113/gsecongeo.81.4.889

Erickson, B. E., and Helz, G. R. (2000). Molybdenum(VI) speciation in sulfidic waters:. *J. Geochimica Cosmochimica Acta* 64 (7), 1149–1158. doi:10.1016/s0016-7037(99)00423-8

French, K. L., Birdwell, J. E., and Whidden, K. J. (2019). Geochemistry of a thermally immature Eagle Ford Group drill core in central Texas. *Org. Geochem.* 131, 19–33. doi:10.1016/j.orggeochem.2019.02.007

Gao, J., Li, X., Cheng, G., Luo, H., and Zhu, H. (2023). Structural evolution and characterization of organic-rich shale from macroscopic to microscopic resolution: the significance of tectonic activity. *Adv. Geo-Energy Res.* 10 (2), 84–90. doi:10.46690/ager.2023.11.03

Ge, X. Y., Mou, C. L., Yu, Q., Liu, W., Men, X., He, J. L., et al. (2021). Discussion on organic matter enrichment in black shales of Wufeng-Longmaxi Formation, eastern Sichuan Basin. *Sediment. Tethys Geol.* 41 (03), 418–435. doi:10.19826/j.cnki.1009-3850.2020.12001

Grygar, T. M., Hošek, M., Mach, K., Schnabl, P., and Martinez, M. (2017). Climatic instability before the miocene climatic optimum reflected in a central European lacustrine record from the most Basin in the Czech republic. *Palaeogeogr. Palaeoclimatol. Palaeoecol.* 485, 930–945. doi:10.1016/j.palaeo.2017.08.011

Guo, T., and Zhang, H. (2014). Formation and enrichment mode of Jiaoshiba shale gas field, Sichuan Basin. *Petrol. Explor. Dev.* 41 (1), 31–40. doi:10.1016/S1876-3804(14)60003-3

Guo, T. L. (2016). Discovery and characteristics of the Fuling shale gas ffeld and its enlightenment and thinking. *Earth Sci. Front.* 23 (2), 317–326. doi:10.13745/j.esf.2016.01.003

Guo, W., Deng, S., and Sun, Y. (2024). Recent advances on shale oil and gas exploration and development technologies. *Adv. Geo-Energy Res.* 11 (2), 81–87. doi:10.46690/ager.2024.02.01

Han, Y., Cao, Y. C., Lian, C., Wu, W., Zhu, Y.Q., Wu, J., et al. (2024). Sedimentary environment evolution of Wufeng-Longmaxi Formation and its control on shale development in southern Sichuan. *J. China Univ. Petroleum Nat. Sci. Ed.* (02), 11–23. doi:10.3969/j.issn.1673-5005.2024.02.002

Hao, F., Zhou, X., Zhu, Y., and Yang, Y. (2011). Lacustrine source rock deposition in response to co-evolution of environments and organisms controlled by tectonic subsidence and climate, Bohai Bay Basin, China. *China. Org. Geochem*. 42, 323–339. doi:10.1016/j.orggeochem.2011.01.010

Hatch, J. R., and Leventhal, J. S. (1992). Relationship between inferred redox potential of the depositional environment and geochemistry of the Upper Pennsylvanian (Missourian) Stark Shale Member of the Dennis Limestone, Wabaunsee County, Kansas, U.S.A. *Chem. Geol.* 99 (1–3), 65–82. doi:10.1016/0009-2541(92)90031-Y

He, L. (2020). Organic matter enrichment and evolution ofsedimentary environment of the Wufeng-Longmaxi shalein southeastern margins of the Sichuan Basin. Guangzhou: University of Chinese Academy of Sciences (Guangzhou Institute of Geochemistry, Chinese Academy of Sciences). doi:10.27544/d.cnki.gzcds.2020.000003

Hu, Z. Q., Du, W., Zhu, T., and Liu, Z.Q. (2022). Sequence stratigraphy and lithofacies characteristics of fine-grained deposits of Wufeng-Longmaxi Formations in the Sichuan Basin and on its periphery. *J. Oil and Gas Geol.* 43 (5), 1024–1038. doi:10.11743/ogg20220502

Huang, Z. S., Wang, X. Z., Yang, X. Y., Zhu, R. K., Cui, J. W., Lu, Y. Z., et al. (2021). Constraints of sedimentary environment on organic matter accumulation in shale: A case study of the Wufeng-Longmaxi formations in the southern Sichuan Basin. *Acta Sedimentol. Sin.* 39 (3), 631–644. doi:10.14027/j.issn.1000-0550.2020.120

Ibad, S. M., and Padmanabhan, E. (2020). Major, trace, and rare earth element geochemistry of black shales from Devonian Sanai Formation in Northwestern Peninsula Malaysia: implications for the depositional environment, provenance, and tectonic setting. *IOP Conf. Ser. Earth Environ. Sci.* 1003 (1), 012023. doi:10.1088/1755-1315/1003/1/012023

Jarvie, D. M., Hill, R. J., Ruble, T. E., and Pollastro, R. M. (2007). Unconventional shale-gas systems: The Mississippian Barnett Shale of north-central Texas as one model for thermogenic shale-gas assessment. *AAPG Bull.* 91 (4), 475–499. doi:10.1306/12190606068

Jiang, P. F., Wu, J. F., Zhu, Y. Q., Zhang, D.K., Wu, W., Zhang, R., et al. (2023). Enrichment conditions and favorable areas for exploration and development of marine shale gas in Sichuan Basin. J. *Acta Pet. Sin.* 44 (1), 91–109. doi:10.7623/syxb202301006

Jin, Z. (2023). Hydrocarbon accumulation and resources evaluation: Recent advances and current challenges. *Adv. Geo-Energy Res.* 8 (1), 1–4. doi:10.46690/ager.2023.04.01

Jones, B., and Manning, D. A. C. (1994). Comparison of geochemical indices used for the interpretation of palaeoredox conditions in ancient mudstones. *Chem. Geol.* 111 (1–4), 111–129. doi:10.1016/0009-2541(94)90085-X

Kimura, H., and Watanabe, Y. (2001). Oceanic anoxia at the Precambrian-Cambrian boundary. *J. Geol.* 29, 995–998. doi:10.1130/0091-7613(2001)029<0995:oaatpc>2.0.co;2

Konert, G. (2001). Paleozoic Stratigraphy and Hydrocarbon Habitat of the Arabian Plate, 2001.

Lerman, A. (1978). *Lakes: Chemistry, Geology, Physics*. New York, NY: Springer-Verlag Berlin Heidelberg, 10–100. doi:10.1007/978-1-4757-1152-3

Li, N., Li, C., Algeo, T. J., Cheng, M., Jin, C., Zhu, G., et al. (2021). Redox changes in the outer Yangtze Sea (South China) through the Hirnantian Glaciation and their implications for the end-Ordovician biocrisis. J. *Earth-Science Rev.* (212), 103443. doi:10.1016/j.earscirev.2020.103443

Li, Y. F., Zhang, T. W., Ellis, G. S., and Shao, D. Y. (2017). Depositional environment and organic matter accumulation of Upper Ordovician— Lower Silurian marine shale in the upper Yangtze platform, South China. *Palaeogeography Palaeoclimatology Palaeoecology*, 466, 252. doi:10.1016/j.palaeo.2016.11.037

Liang, C. (2015). *The sedimentation and reservoir formation mechanism of hydrocarbon-bearing fine-grained sedimentary rocks*. Beijing: China University of Geosciences. Available online at: https://kns.cnki.net/kcms2/article/abstract.

Liang, C., Jiang, Z. X., Yang, Y. T., and Wei, X. J. (2012). Shale lithofacies and reservoir space of the Wufeng–Longmaxi formation, Sichuan basin, China. *Petrol. Explor. Dev.* 39, 736–743. doi:10.1016/S1876-3804(12)60098-6

Liang, C., Wu, J., Jiang, Z., Cao, Y., and Song, G. (2018). Sedimentary environmental controls on petrology and organic matter accumulation in the upper fourth member of the Shahejie Formation (Paleogene, Dongying depression, Bohai Bay Basin, China). *Int. J. Coal Geol.* 186, 1–13. doi:10.1016/j.coal.2017.11.016

Liu, T., Feng, M. Y., Wang, X. Z., Chen, B., Zhang, L.H., Liu, X. H., et al. (2019). Geochemical characteristics of Late Ordovician Wufeng elements and their constraints on sedimentary environment in Wuxi area, northeast Chongqing. *Nat. Gas. Geosci.* (05), 740–750. doi:10.11764/i.issn.1672-1926.2019.01.012

Liu, W., Zhang, C., Gao, G., Luo, C., Wu, W., Shi, X., et al. (2017). Controlling factors and evolution laws of shale porosity in Longmaxi Formation, Sichuan Basin. *Acta Pet. Sin.* 38 (02), 175–184. doi:10.7623/syxb201702005

Liu, Y. D., Liang, C., Cao, Y. C., Wu, J., Han, Y., Xie, H. Y., et al. (2023). Shale lithofacies characteristics and sedimentation of Wufeng-Longmaxi Formation in southern Sichuan. *Acta Sedimentol. Sin.*, 1–24. doi:10.14027/j.issn.1000-0550.2022.153

Liu, Z. Q., Zhao, S. H., Hu, Z. Q., Shen, B.J., Feng, D.J., Zhang, J.Q., et al. (2025). Characteristics and controlling factors of coal-measure unconventional reservoirs – a case study of the Carboniferous-Permian in the Ordos Basin. Unconventional Resources.

Lu, J. K., Zhai, S. K., Yu, Z. H., Liu, X. F., and Wang, K. (2021). Application and influence factors of redox-sensitive elements in a sedimentary environment. *Mar. Sci.* 45 (12), 108–124. doi:10.11759/hykx20210712002

Lu, Y., Hao, F., Lu, Y., Yan, D., Xu, S., Shu, Z., et al. (2020). Lithofacies and depositional mechanisms of the Ordovician–Silurian Wufeng–Longmaxi organic-rich shales in the Upper Yangtze area, southern China. *Aapg Bull.* 104 (1), 97–129. doi:10.1306/04301918099

Lüning, S., Craig, J., Loydell, D. K., Štorch, P., and Fitches, B. (2000). Lower Silurian 'hot shales' in North Africa and Arabia: regional distribution and depositional model. *Earth-Sci. Rev*. 49 (1-4), 121–200. doi:10.1016/S0012-8252(99)00060-4

Lüning, S., Shahin, Y. M., Loydell, D., Al-Rabi, H. T., Masri, A., Tarawneh, B., et al. (2005). Anatomy of a world-class source rock: distribution and depositional model of Silurian organic-rich shales in Jordan and implications for hydrocarbon potential. *AAPG (Am. Assoc. Pet. Geol.) Bull.* 89 (10), 1397–1427. doi:10.1306/05250505014

Ma, Y. Q., Fan, M. J., Lu, Y. C., Guo, X. S., Hu, H. Y., Chen, L., et al. (2016). Geochemistry and sedimentology of the lower Silurian Longmaxi mudstone in southwestern China: implications for depositional controls on organic matter accumulation. *Mar. and Petroleum Geol.* 75, 291–309. doi:10.1016/j.marpetgeo.2016.04.024

Mahmoud, M. D., Vaslet, D., and Husseini, M. I. (1992). The lower Silurian Qalibah formation of Saudi Arabia: an important hydrocarbon source rock 1. AAPG (Am. Assoc. Pet. Geol.) Bull. 76 (10), 1491–1506. doi:10.1306/BDFF8A24-1718-11D7-8645000102C1865D

Mao, X. P., Chen, X. R., Wang, Z. J., Yang, Y. X., Li, S. X., and Yang, F. (2024). The relationship between organic matter enrichment and paleo-climate in black shales: a case study of the Wufeng-Longmaxi Formation shales in the Middle and Upper Yangtze. *Sci. Geol.* (05), 1151–1172.

Nie, H. K., Jin, Z. J., Ma, X., Liu, Z. B., Lin, T., and Yang, Z. H. (2017). Graptolites zone and sedimentary characteristics of Upper Ordovician Wufeng Formation—Lower Silurian Longmaxi Formation Sichuan basin and its adjacent areas. *Acta Pet. Sin.* 38 (2), 160–174. doi:10.7623/syxb201702004

Piper, D. Z., and Dean, W. E. (2002). Trace-element deposition in the Cariaco Basin, Venezuela Shelf, Under sulfate-reducing conditions—a history of the local hydrography and global climate, 20 Ka to the present. *Cent. Integr. Data Anal. Wis. Sci. Cent.* 1–41.

Plint, A. G. (2014). Mud dispersal across a Cretaceous prodelta: Storm-generated, wave-enhanced sediment gravity flows inferred from mudstone microtexture and microfacies. *Sedimentology* 61 (3), 609–647. doi:10.1111/sed.12068

Potter, C. J. (2018). Paleozoic shale gas resources in the Sichuan Basin, China. *Am. Assoc. Pet. Geol. Bull.* 102 (6), 987–1009. doi:10.1306/0828171607817072

Qin, H. X., Chen, L., Lu, C., Hu, Y., Xiong, M., Tan, X. C., et al. (2024). Geochemical characteristics of shale in Wufeng-Longmaxi Formation, southern margin of Yangzi and their implications for weathering, provenance and tectonic setting. *Geol. LunPing* (4), 1314–1334. doi:10.16509/j.g.eoreview.2024.01.002

Qiu, Z., Jiang, Z. G., Dong, D. Z., Shi, Z.S., Lu, B., Tan, X., et al. (2017). Organic matter enrichment model of the shale in Wufeng-Longmachi Formation of Wuxi area. *J. China Univ. Min. and Technol.* 46 (5), 1134–1143. doi:10.13247/j.cnki.jcumt.000674

Ran, B., Liu, S. G., Jansa, L., Sun, W., Yang, D., Ye, Y., et al. (2015). Origin of the Upper Ordovician—Lower Silurian cherts of the Yangtze Block, South China, and their palaeogeographic significance. *J. Asian Earth Sci.* 108, 1–17. doi:10.1016/j.jseaes.2015.04.007

Rimmer, S. M. (2004). Geochemical paleoredox indicators in Devonian–Mississippian black shales, central Appalachian Basin (USA). *Chem. Geol.* 206 (3-4), 373–391. doi:10.1016/j.chemgeo.2003.12.029

Rimmer, S. M., Thompson, J. A., Goodnight, S. A., and Robl, T. L. (2004). Multiple controls on the preservation of organic matter in Devonian–Mississippian marine black shales: geochemical and petrographic evidence. *Palaeogeogr. Palaeoclimatol. Palaeoecol.* 215, 125–154. doi:10.1016/s0031-0182(04)00466-3

Ross, D. J., and Bustin, R. M. (2009). Investigating the use of sedimentary geochemical proxies for paleoenvironment interpretation of thermally mature organic-rich strata: Examples from the Devonian–Mississippian shales, Western Canadian Sedimentary Basin. *Chem. Geol.* 260 (1-2), 1–19. doi:10.1016/j.chemgeo.2008.10.027

Sen, S., and Kozlu, H. (2020). Impact of maturity on producible shale oil volumes in the Silurian (Llandovery) hot shales of the northern Arabian plate, southeastern Turkey. *AAPG Am. Assoc. Pet. Geol. Bull.* 104 (3), 507–524. doi:10.1306/05141917201

Smolarek, J., Trela, W., Bond, D. P., and Marynowski, L. (2017). Lower Wenlock black shales in the northern Holy Cross Mountains, Poland: sedimentary and geochemical controls on the Ireviken Event in a deep marine setting. *Geol. Mag.* 154 (2), 247–264. doi:10.1017/S0016756815001065

Tan, C. (2017). *Sedimentary characteristics and paleoclimate evolution of upper permian-middle-upper triassic in ordos basin*. Beijing: China University of Geosciences.

Tang, D. J., Shi, X. Y., Zhao, X. K., Wang, X. Q., and Song, G. Y. (2019). Mo-U covariation as an important proxy for sedimentary environment redox conditions-progress, problems and prospects. *J. Geosci.* 29 (1), 1–13. doi:10.3969/j.issn.1000-8527.2015.01.001

Taylor, S. R., and McLennan, S. M. (1985). The continental crust: its composition and evolution.

Torsvik, T. H., and Cocks, L. R. M. (2013). Gondwana from top to base in space and time. *Gondwana Res.* 24(3-4), 999–1030. doi:10.1016/j.gr.2013.06.012

Tribovillard, N., Algeo, T. J., Baudin, F., and Riboulleau, A. J. C. G. (2012). Analysis of marine environmental conditions based onmolybdenum–uranium covariation—Applications to Mesozoic paleoceanography. *J. Chem. Geol.* 324, 46–58. doi:10.1016/j.chemgeo.2011.09.009

Tribovillard, N., Algeo, T. J., Lyons, T., and Riboulleau, A. (2006). Trace metals as paleoredox and paleoproductivity proxies: An update. *Chem. Geology* 232 (1-2), 12–32. doi:10.1016/j.chemgeo.2006.02.012

Wang, A. L., Wang, Z. H., Liu, J. H., Xu, N. C., and Li, H. L. (2021). The Sr/Ba ratio response to salinity in clastic sediments of the Yangtze River Delta. *J. Chem. Geol.* 559, 1–15. doi:10.1016/j.chemgeo.2020.119923

Wang, C., Zhang, B. Q., Shu, Z. G., Lu, Y. C., Lu, Y. Q., Bao, H. Y., et al. (2018). Lithofacies types and reservoir characteristics of marine shales of the Wufeng Formation-Longmaxi Formation in Fuling area, the Sichuan Basin. *Oil and Gas Geol.* 39 (3), 485–497. doi:10.11743/ogg20180306

Wang, F., Liu, X. C., Deng, X. Q., Li, Y. H., Tian, J. C., Li, S. X., et al. (2017). Geochemical Characteristics and Environmental Implications of Trace Elements of Zhifang Formation in Ordos Basin. *Acta Sedimentol. Sin.* 35 (6), 1265–1273. doi:10.14027/j.cnki.cjxb.2017.06.017

Wang, R. Y., Hu, Z. Q., Hu, Z. Q., Liu, G. X., Xi, B. B., and Liu, W. X. (2020). Controlling effect of pressure evolution on shale gas reservoirs: A case study of the Wufeng–Longmaxi Formation in the Sichuan Basin. *Nat. Gas. Ind.* 40 (10), 1–11. doi:10.11781/sysydz202106996-en

Wang, R. Y., Hu, Z. Q., Bao, H. Y., Wu, J., Du, W., Wang, P.W., et al. (2021a). Diagenetic evolution of key minerals and its controls on reservoir quality of Upper Ordovician Wufeng-Lower Silurian Longmaxi shale of Sichuan Basin. *Pet. Geol. Exp.* 43 (6), 996–1005. doi:10.11781/sysydz202106996-en

Wang, R. Y., Hu, Z. Q., Dong, L., Gao, B., Sun, C. X., Yang, T., et al. (2021b). Advancement and trends of shale gas reservoir characterization and evaluation. *Oil and Gas Geol.* 42 (1), 54–65. doi:10.11743/ogg20210105

Wang, R. Y., Hu, Z. Q., Zhou, T., Bao, H. Y., Wu, J., Du, W., et al. (2021c). Characteristics of fractures and their significance for reservoirs in Wufeng-Longmaxi shale, Sichuan Basin and its periphery. *Oil and Gas Geol.* 42(6), 1295–1306. doi:10.1111/1755-6724.13875

Wang, R. Y., Hu, Z. Q., Long, S. X., Du, W., Wu, J., Wu, Z. H., et al. (2022). Reservoir characteristics and evolution mechanisms of the Upper Ordovician Wufeng-Lower Silurian Longmaxi shale, Sichuan Basin. *J. Oil and Gas Geol.* 43 (2), 353–364. doi:10.11743/ogg20220209

Wang, T., Zhu, X. M., Dong, Y. L., Chen, H. H., Su, B., Liu, Y., et al. (2020). Trace elements as paleo sedimentary environment indicators: a case study of the Paleogene Anjihaihe Formation in the northwestern Junggar Basin. *J. Acta Geol. Sin.* 94 (12), 3830–3851. doi:10.19762/j.cnki.dizhixuebao.2020045

Wang, X., Tian, J. C., Lin, X. B., Chen, W. Z., and Yi, D. X. (2024). Sedimentary environment and controlling factors of organic matter accumulation in wufeng-longmaxi formations: A case study of Jielong section in eastern Chongqing. *Acta Sedimentol. Sin.*. doi:10.14027/j.issn.1000-0550.2022.069

Wang, Y. Y., Guo, W. Y., and Zhang, G. D. (1979). Application of some geochemical indicators in determining of sedimentary environment of the funing group(paleogene), Jin-Hu Depression, Kiangsu Province. *J. Tongji Univ.* 02, 51–60. Available online at: https://kns.cnki.net/kcms2/article/abstract.

Wang, Y., Liu, L. F., Zheng, S. S, Luo, Z. H., Sheng, Y., and Wang, X. M. (2019). Full-scale pore structure and its controlling factors of the Wufeng-Longmaxi shale, southern Sichuan Basin, China: Implications for pore evolution of highly overmature marine shale. *J. Nat. Gas Sci. Eng.* 67, 134–146. doi:10.1016/j.jngse.2019.04.020

Wang, Z. G. (2015). Breakthrough of Fuling shale gas exploration and development and its inspiration. *Oil and Gas. Geol.* 36. doi:10.11743/ogg20150101

Wedepohl, K. H. (1971). Environmental influences on the chemical composition of shales and clays. *Phys. Chem. Earth* 8 (71), 307–333. doi:10.1016/0079-1946(71)90020-6

Wei, C., Dong, T., He, Z. L., He, S., He, Q., Yang, R., et al. (2021). Major, trace-elemental and sedimentological characterization of the upper Ordovician Wufeng-lower Silurian Longmaxi formations, Sichuan Basin, South China: Insights into the effect of relative sea-level fluctuations on organic matter accumulation in shales. *J. Mar. Petroleum Geol.* 126, 104905. doi:10.1016/j.marpetgeo.2021.104905

Wei, H. Y. (2012). Paleomarine productivity and redox indices: a review of elemental geochemistry. *Sediment. Tethian Geol.*, (02) 76–88.

Wen, H. G., Zheng, R. C., Tang, F., Zheng, A. P., Sang, Y. Y., Chen, S. C., et al. (2008). Paleosalinity restoration and paleoenvironment analysis of Chang 6 Member in Gengwan Area, Ordos Basin. *Mineral. Rock* (01), 114–120. doi:10.19719/j.carolcarrollnki.1001-6872.2008.01.016

Westermann, S., Stein, M., Matera, V., Fiet, N., Fleitmann, D., Adatte, T., et al. (2013). Rapid changes in the redox conditions of the western Tethys Ocean during the early Aptian oceanic anoxic event. *J. Geochimica Cosmochimica Acta* 121, 467–486. doi:10.1016/j.gca.2013.07.023

Xia, P., Hao, F., Yang, C., Tian, J., Fu, Y., and Wang, K. (2024). Mechanism of organo-nickel co-enrichment in marine black shale. *Adv. Geo-Energy Res.* 13 (1), 10–21. doi:10.46690/ager.2024.07.03

Xiao, B. (2019). The sichuan basin north rim five mountains - the dragon stream group black shale dominative factor organic matter enrichment in research (Ph.D. Dissertation, Chengdu University of Technology). doi:10.26986/d.cnki.gcdlc.2019.001114

Xu, H., Zhou, W., Hu, Q. H., Yi, T., Ke, J., Zhao, A. K., et al. (2021). Quartz types, silica sources and their implications for porosity evolution and rock mechanics in the Paleozoic Longmaxi Formation shale, Sichuan Basin. *Mar. Petroleum Geol.* 128, 105036. doi:10.1016/j.marpetgeo.2021.105036

Xu, S., Wang, S. W., and Yang, J. C. (2022). Implications of Graptolite Characteristics in Black Shale in Southeast Sichuan on Shale Gas Generation and Storage. *Value Eng.* 41 (31). doi:10.3969/j.issn.1006-4311.2022.31.049

Xu, Y. J., and Du, Y. S. (2018). From periphery collision to intra plate orogeny:Early Paleozoic orogenesis in southeastern part of South China. *Earth Sci.* 43 (2), 333–353. doi:10.3799/dqkx.2017.582

Yang, X. R., Yan, D. T., Wei, X. S., Zhang, L. W., Zhang, B., Xu, H. W., et al. (2018). Different Formation mechanism of quartz in siliceous and argillaceous shales: A case study of Longmaxi Formation in South China. Marine and Petroleum. *Geology* 94, 80–94. doi:10.1016/j.marpetgeo.2018.03.036

Zhang, C., Wang, L., Li, G., Dong, S., Yang, J., and Wang, X. (2002). Grain size effect on multi-element concentrations in sediments from the intertidal flats of Bohai Bay, China. *Appl. Geochem.* 17 (1), 59–68. doi:10.1016/S0883-2927(01)00079-8

Zhang, C. C., Wang, Y. M., Dong, D. Z., and Guan, Q. Z. (2016). Brittleness characteristics of Wufeng-Longmaxi shale in Changning region, southern Sichuan, China. *Nat. Gas. Geosci.* 27 (9), 1629–1639. doi:10.11764/j.issn.1672-1926.2016.09.1629

Zhang, H. (2015). *Optimisation of shale gas production capacity construction targets of Longmaxi Formation in Weiyuan area, Sichuan Basin*. Master's Thesis, Southwest Petroleum University.

Zhang, J., Li, X., Zhang, X., Zhang, M., Cong, G., Zhang, G., et al. (2018). Geochemical and geological characterization of marine–continental transitional shales from Longtan Formation in Yangtze area, South China. *Mar. Petroleum Geol.* 96, 1–15. doi:10.1016/j.marpetgeo.2018.05.020

Zhang, J. C., Xu, B., Nie, H. K., Wang, Z. Y., Lin, T., Jiang, S. L., et al. (2008). Exploration potential of shale gas resources in China. *Nat. Gas. Ind.* 6, 136–140. doi:10.3787/j.issn.1000-0976.2021.01.002

Zhang, L. C., Xiao, D. S., Lu, S. F., Jiang, S., and Lu, S. D. (2019). Effect of sedimentary environment on the Formation of organic-rich marine shale: insights from major/trace elements and shale composition. *Int. J. Coal Geol.* 204, 34–50. doi:10.1016/j.coal.2019.01.014

Zhang, M. L., Guo, W., Shen, J., Liu, K., Zhou, L., Feng, Q. L., et al. (2017). New progress in the study of paleo-ocean redox geochemical indicators. *Geol. Sci. Technol. Inf.* 36 (4), 95–106. doi:10.19509/j.cnki.dzkq.2017.0412

Zhang, Q., Littke, R., Zieger, L., Shabani, M., Tang, X., and Zhang, J. (2019). Ediacaran, Cambrian, Ordovician, Silurian and Permian shales of the Upper Yangtze Platform, South China: Deposition, thermal maturity and shale gas potential. *Int. J. Coal Geol.* 216, 103281. doi:10.1016/j.coal.2019.103281

Zhao, L., Mao, W., Liu, Z., and Cheng, S. (2023). Research on the differential tectonic-thermal evolution of Longmaxi shale in the southern Sichuan Basin. *Adv. Geo-Energy Res.* 7 (3), 152–163. doi:10.46690/ager.2023.03.02

Zhao, L., Zhao, Y., Yan, D., Zhu, J., and Cai, J. (2024). Integrated rock physics characterization of unconventional shale reservoir: A multidisciplinary perspective. *Adv. Geo-Energy Res.* 14 (2), 86–89. doi:10.46690/ager.2024.11.02

Zhou, K. K., Mou, C. L., Xu, X. S., Ge, X. Y., and Liang, W. (2014). Early Silurian paleogeography and source—reservoir—cap rocks of the middle—upper Yangtze region in South China. *Petroleum Explor. and Dev.* 41 (5), 684–694. doi:10.1016/S1876-3804(14)60082-3

Zhou, L., Su, J., Huang, J. H., Yan, J. X., Xie, X. N., Gao, S., et al. (2011). A new paleoenvironmental index for anoxic events-Mo isotopes in black shales from Upper Yangtze marine sediments. *J. Sci. China Earth Sci.* 54, 1024–1033. doi:10.1007/s11430-011-4188-z

Zhu, H. J., Ju, Y. W., Lu, Y. N., Yang, M. P., Feng, H. Y., Qiao, P., et al. (2025). Natural evidence of organic nanostructure transformation of shale during bedding-parallel slip. *Geol. Soc. Am. Bull.* 137, 2719–2746. doi:10.1130/B37712.1

Zhu, H. J., Lu, Y. J., Pan, Y. Y., Qiao, P., Raza, A., and Liu, W. (2024). Nanoscale mineralogy and organic structure characterization of shales: Insights via AFM-IR spectroscopy. *Adv. Geo-Energy Res.* 13 (3), 231–236. doi:10.46690/ager.2024.09.08

Zou, C. N., Qiu, Z., Poulton, S. W., Dong, D. Z., Wang, H. Y., Chen, D. Z., et al. (2018). Ocean euxinia and cli mate change "double whammy" drove the Late Ordovician mass extinction. *Geology* 46 (6), 535–538. doi:10.1130/g40121.1

Zou, X. Y., Li, X. Q., Wang, Y., Zhang, J. Z., and Zghao, P. (2022). Reservoir characteristics and gas content of Wufeng-Longmaxi formations deep shale in southern Sichuan Basin. *Nat. Gas. Geosci.* 33 (4), 654–665. doi:10.11764/j.issn.1672-1926.2021.10.004